

23583

SIMULATION OF UNCODED AND CONVOLUTIONALLY ENCODED
CONTINUOUS PHASE FREQUENCY SHIFT KEYED SIGNALS BY USING
SIGNAL SPACE METHOD

A Master's Thesis

Presented by

Ahmet Gürkan SANCAR

to

the Graduate School of Natural and Applied Sciences
of Middle East Technical University
in Partial Fulfillment for the Degree of

MASTER OF SCIENCE

in

ELECTRICAL AND ELECTRONICS ENGINEERING

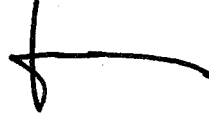
MIDDLE EAST TECHNICAL UNIVERSITY

ANKARA

September, 1992

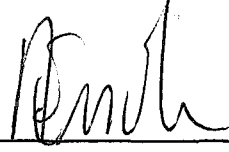
**T.C. YÜKSEKÖĞRETİM KURULU
DOKÜMANTASYON MERKEZİ**

Approval of the Graduate School of Natural and Applied
Sciences



Prof. Dr. Alpay ANKARA
Director

I certify that this thesis satisfies all the requirements
as a thesis for the degree of Master of Science.



Prof. Dr. Tuncay Birand
Chairman of the Department

We certify that we have read this thesis and that in our
opinion it is fully adequate, in scope and quality, as a
thesis for the degree of Master of Science in Electrical
and Electronics Engineering.



Assoc. Prof. Dr. Melek D. YÜCEL
Supervisor

Examining Committee in Charge:

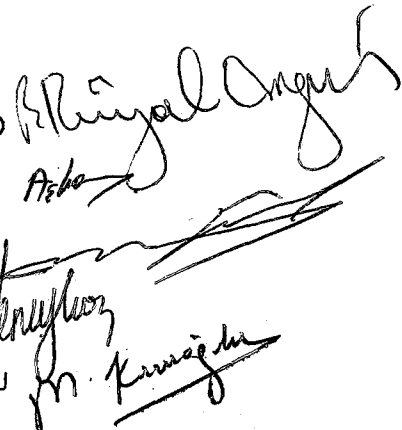
Prof. Dr. Rüyal ERGÜL (Chairman)

Prof. Dr. Murat AŞKAR

Assoc. Prof. Dr. Melek D. YÜCEL

Asst. Prof. Dr. Sencer KOÇ

Asst. Prof. Dr. Mustafa KUZUOĞLU



ABSTRACT

SIMULATION OF UNCODED AND CONVOLUTIONALLY ENCODED
CONTINUOUS PHASE FREQUENCY SHIFT KEYED SIGNALS BY USING
SIGNAL SPACE METHOD

SANCAR, Ahmet Gürkan

M.S. in Electrical and Electronics Engineering

Supervisor: Assoc. Prof. Dr. Melek D. YÜCEL

September, 1992, 83 pages.

In this study, some uncoded and convolutionally encoded continuous phase frequency shift keying (CPFSK) systems are studied. It is assumed that the channel is an additive white Gaussian noise channel and the noise is introduced to the modulated signals by the so called signal space method, for which an orthonormal basis is derived. It is assumed that the receiver performs coherent maximum likelihood sequence detection by means of the Viterbi algorithm. The bit error probability of the simulated systems are obtained and, it is observed that several decibels of signal to noise ratio gain can be obtained by convolutionally encoding the CPFSK

signals. The orthonormal basis and the table obtained for modulating signals can be used for any rate $1/2$ convolutional encoder combined with CPFSK system.

Keywords: Continuous Phase Modulation, Continuous Phase Frequency Shift Keying, Signal Space Method, Convolutional Encoding, Viterbi Algorithm

Science Code: 609.02.07



02

SINYAL UZAYI YÖNTEMİ KULLANILARAK KODLANMAMIŞ VE EVRİŞİM
KODLU FREKANS KAYDIRIP ANAHTARLANAN SÜREKLİ FAZ
SINYALLERİNİN BENZETİMİ

SANCAR, Ahmet Gürkan

Yüksek Lisans Tezi, Elektrik ve Elektronik Mühendisliği

Anabilim Dalı

Tez Yöneticisi: Doç.Dr.Melek D.YÜCEL

Eylül, 1992, 83 sayfa

Bu çalışmada, bazı kodlanmamış ve evrişim kodlu frekans kaydırıp anahtarlanan sürekli faz sinyalleri sistemi üzerinde çalışıldı. Kanalin toplanır, beyaz, Gauss gürültüsü kanalı olduğu varsayıldı ve kiplenmiş sinyallere sinyal uzayı yöntemi kullanılarak gürültü eklendi. Bu yöntem için dikdüzgölü bir baz çıkarıldı. Alıcının Viterbi algoritması kullanarak bağımsız en yüksek olasılık sezimi yaptığı varsayıldı. Benzetimi yapılan sistemlerin ikil hata olasılığı elde edildi ve evrişim kodları kullanılarak bir kaç desibel işaret gürültü oranı kazancı elde edilebildiği görüldü. Elde edilen dikdüzgölü baz ve kiplenmiş sinyal tablosu, bütün 1/2 oranlı evrişim kodlu frekans kaydırıp anahtarlanan sürekli faz sinyalleri için kullanılabilir.

Anahtar Kelimeler : Sürekli Faz Kiplemesi, Frekans Kaydırıp
Anahtarlanan Sürekli Faz Kiplemesi, Sinyal Uzayı Yöntemi,
Evrişim Kodları, Viterbi Algoritması.

Bilim Dalı Sayısal Kodu : 609.02.07



ACKNOWLEDGEMENTS

I would like to thank Assoc.Prof.Dr.Melek D.Yücel for precious contribution and help that she kindly provided throughout this work.



TABLE OF CONTENTS

	Page
ABSTRACT	iii
ØZ	v
ACKNOWLEDGEMENTS	vii
LIST OF TABLES	xi
LIST OF FIGURES	xii
LIST OF SYMBOLS	xiv
CHAPTER I: INTRODUCTION	1
CHAPTER II: CONTINUOUS PHASE MODULATION SYSTEMS	4
2.1 Continuous Phase Modulation	4
2.1.1 State Description of CPM	6
2.2 Convolutionally Encoded CPM	8
2.2.1 Convolutional Codes	10
2.2.2 State Description of Convolutionally Encoded CPM	11
2.3 Transmission of CPM	12
2.3.1 Basic Quadrature Transmitter	13
2.4 Receivers for CPM	14
2.4.1 Viterbi Receiver for Conventional CPM	14
2.5 Error Performance	16

CHAPTER III: UNCODED AND ENCODED CPFSK SCHEMES	18
3.1 Introduction	18
3.2 Minimum Normalized Squared Euclidean Distance ...	18
3.3 The Effect of Channel Noise	25
3.3.1 Signal Space Method	27
3.4 Uncoded CPFSK	28
3.4.1 The Viterbi Algorithm and the Simulation	32
3.5 Simulation of Convolutionally Encoded CPFSK with R=1/2, (7,2) code	37
3.5.1 Orthonormal Functions and Vector Representation of the Transmitted Signals ...	38
3.5.2 The Modified Viterbi Algorithm and System Simulation	44
3.6 Simulation Results	47
CHAPTER IV: CONCLUSION	53
REFERENCES	56

APPENDICES

APPENDIX A. DISTANCE CALCULATIONS FOR THE TWO PATH GIVEN IN FIGURE 3.2 FOR SEVERAL MODULATION INDICES	59
A.1 Calculation of $d_{12}^2(4)$ for the Two Path Given in Figure 3.2 for $h=3/10$	59

A.2 Calculation of $d_{12}^2(4)$ for the Two Path Given in
Figure 3.2 for $h=1/4$ 60

A.3 Calculation of $d_{12}^2(4)$ for the Two Path Given in
Figure 3.2 for $h=1/6$ 61

APPENDIX B. DERIVATION OF THE 8 AND 4 DIMENSIONAL
ORTHONORMAL BASIS FOR MODULATING SIGNALS ..63



LIST OF TABLES

	Page
Table 3.1 MNSSED and Minimum Distance Event Length Table for (7,2) Coded CPFSK	25
Table 3.2 Coefficients for the Signal Vectors for Uncoded 2 Level CPFSK	31
Table 3.3 All Transmitted Signal Space Vectors for h=1/2 Uncoded CPFSK	33
Table 3.4 All Transmitted Signal Space Vectors for h=1/4 Uncoded CPFSK	34
Table 3.5 The Relation Between the Generated Bits and the Output Bit of the 4-Level Mapper ...	39
Table 3.6 Coefficients for the Transmitted Signal Vectors for R=1/2 (7,2) Convolutionally Encoded CPFSK	43

LIST OF FIGURES

	Page
Figure 2.1. The Conventional CPM System	5
Figure 2.2. Convolutionally Encoded CPM System	8
Figure 2.3. Basic Quadrature Transmitter	12
Figure 3.1. Rate 1/2 (7,2) Convolutional Encoder and Four Level Mapper	21
Figure 3.2. Corresponding Phase Tree When Rate 1/2 (7,2) Convolutional Encoder and Four- Level Mapper	22
Figure 3.3. General CPM System with AWGN and with Viterbi Receiver	26
Figure 3.4. The State Trellis Diagram for h=1/2 Uncoded CPFSK	33
Figure 3.5. The State Trellis Diagram for h=1/4 Uncoded CPFSK	34
Figure 3.6. Probability of Error Curve for h=1/2 Uncoded CPFSK with $Q\left[\sqrt{d_{\min}^2 E_b / N_0}\right]$ curve	48
Figure 3.7. Probability of Error Curve for h=1/4 Uncoded CPFSK with $Q\left[\sqrt{d_{\min}^2 E_b / N_0}\right]$ Curve	49

Figure 3.8. Probability of Error Curve for $h=1/4$,
R=1/2 (7,2) Convolutionally Encoded
CPFSK with $Q\left[\sqrt{d_{\min}^2 E_b / N_0}\right]$ curve 50

Figure 3.9. Probability of Error Curve for the
Uncoded and Encoded CPFSK for $h=1/4$ 51



LIST OF SYMBOLS

AWGN	Additive White Gaussian Noise
CPFSK	Continuous Phase Frequency Shift Keying
CPM	Continuous Phase Modulation
MNSED	Minimum Normalized Squared Euclidean Distance
SNR	Signal to Noise Ratio



CHAPTER I

INTRODUCTION

Constant-amplitude digital modulation schemes have been proposed and analyzed in the recent literature. Many of these schemes are special cases of the Continuous Phase Modulation (CPM) class (Aulin et al, 1981 a-b). Memory is introduced into the transmitted signal by means of continuous phase and also by means of correlative encoding. Uncoded partial-response CPM yields good combined power and bandwidth efficiency (Anderson et al, 1986). Continuous Frequency Shift Keying (CPFSK) is a special case of the CPM signal class (Anderson et al, 1986).

In this thesis work, some uncoded and convolutionally encoded CPFSK signalling schemes are studied. Transmission over an additive white Gaussian noise (AWGN) channel is considered. The receiver is an ideal coherent maximum likelihood sequence detector using the Viterbi algorithm both for the uncoded and the encoded cases. In order to simulate the effect of AWGN

channel on the transmitted signals the so called signal space method is used. By this way computation of integrals for metrics of the Viterbi receiver is avoided. To use the signal space method, an orthonormal basis is derived for both the uncoded and convolutionally encoded CPFSK systems. Also for these CPFSK systems, the probability of error performance is obtained by computer simulations.

In chapter 2, continuous phase modulation systems are introduced. The difference between convolutionally encoded CPM and conventional CPM is presented and their state structures are given. Viterbi receiver is used for coherent detection of CPM signals. An approximation is given for the symbol error probability in AWGN channel.

In chapter 3, the simulation of convolutionally encoded and uncoded CPFSK systems are presented. Because of its importance in the probability of error calculations, minimum normalized squared Euclidean distance is introduced and its calculation is explained. Then the signal space method for the simulation of channel noise is presented and a 4-dimensional basis for the uncoded CPFSK for the use of this method is given. The system is simulated for $h=1/2$ and $h=1/4$ uncoded CPFSK and tables for modulating signals are obtained for

these cases.

And then for the convolutionally encoded CPFSK system simulation, an 8 dimensional orthonormal basis is derived to use the signal space method. The system is simulated for $h=1/4$ convolutionally encoded CPFSK with the rate $R=1/2$ (7,2) convolutional encoder and a table for the modulated signals are obtained. The Viterbi algorithm and metric derivations for the algorithm are given for both the uncoded and convolutionally encoded CPFSK systems. The bit error performances of the coded and encoded systems are given, and compared.

In chapter 5, final discussions are made about the results of this study.

CHAPTER II

CONTINUOUS PHASE MODULATION SYSTEMS

In this chapter convolutionally encoded and uncoded Continuous Phase Modulation are explained and general features of them are given.

2.1 Continuous Phase Modulation

Continuous Phase Modulation (CPM) is a bandwidth efficient constant envelope signaling scheme for digital transmission over bandlimited channels. CPM is represented by a signal of the form $A \cos(2\pi f_c t + \phi(t))$ where the phase $\phi(t)$ is continuous and follows some coded pattern in response to data. The conventional CPM system is given in Figure 2.1.

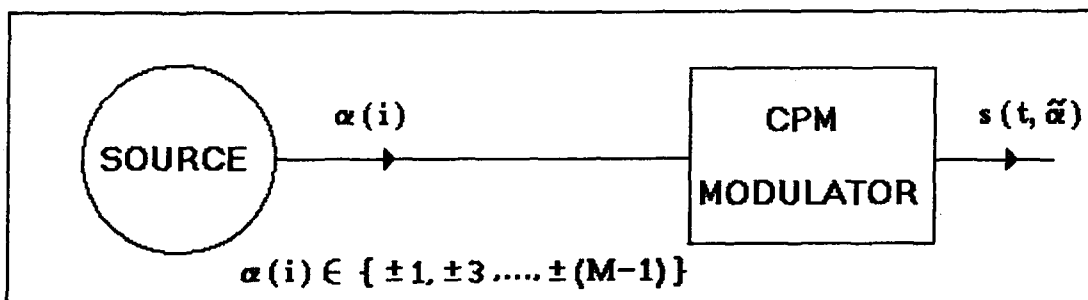


Figure 2.1. The Conventional CPM System

The CPM signal associated with the sequence $\tilde{\alpha} = \dots, \dots, \alpha_{-1}, \alpha_0, \alpha_1, \dots$ chosen from the M-ary alphabet $\{\pm 1, \pm 3, \dots, \pm(M-1)\}$ is

$$S(t, \tilde{\alpha}) = \sqrt{\frac{2E}{T}} \cos(2\pi f_c t + \phi(t, \tilde{\alpha}) + \phi_0) \quad (2.1)$$

where the phase $\phi(t, \tilde{\alpha})$ is

$$\phi(t, \tilde{\alpha}) = \sum_{i=-\infty}^{\infty} \pi h \alpha_i g(t-iT) \quad (2.2)$$

with

$$g(t) = \int_{-\infty}^t f(\tau) d\tau \quad (2.3)$$

ϕ_0 is a constant phase shift, T is the symbol length, and E is the symbol energy. Here h is the modulation index.

The pulse $g(t)$ in (2.3) is called the phase response and is equal to the integral of the baseband pulse $f(t)$. It is assumed that $f(t)$ is strictly time-limited to the interval $[0, LT]$ and the area under $f(t)$ is normalized to unity, so that the maximum phase change caused by the symbol α_n is $\pi h \alpha_n$.

Note that if $f(t)=0$, for $t>T$, the CPM signal is called full response CPM. If $f(t)\neq 0$, for $t>T$, the

modulated signal is called partial response CPM. An infinite variety of CPM signals can be generated by choosing different pulse shapes $f(t)$ and by varying the modulation index h and the alphabet size M .

Generally used pulse shapes for $f(t)$ are the rectangular and raised cosine pulses. An LREC pulse is a rectangular pulse of length LT :

$$f(t) = \begin{cases} \frac{1}{LT} , & 0 \leq t \leq LT \\ 0 , & \text{elsewhere} \end{cases} \quad (2.4)$$

and an LRC pulse is a raised cosine pulse of length LT :

$$f(t) = \begin{cases} \frac{1}{LT} \left[1 - \cos\left(\frac{2\pi}{LT} t\right) \right] , & 0 \leq t \leq LT \\ 0 , & \text{elsewhere} \end{cases} \quad (2.5)$$

Note that CPM modulation with 1REC pulse is also known as Continuous Phase Frequency Shift Keying (CPFSK). And, CPFSK with $h=1/2$ is known as Minimum Shift Keying. Note also that, the modulation index h can be changed for every symbol interval T , so that the so called multi- h CPM signal is obtained.

2.1.1 State Description of CPM

We can rewrite (2.2), the phase relative to the

carrier of the transmitted signal, as

$$\begin{aligned}\phi(t, \tilde{\alpha}_n) &= \sum_{i=-\infty}^n \pi h \alpha_i g(t-iT) \\ &= \pi h \sum_{i=n-L+1}^n \alpha_i g(t-iT) + \pi h \sum_{i=-\infty}^{n-L} \alpha_i, nT \leq t \leq (n+1)T \quad (2.6)\end{aligned}$$

by using the properties that $g(t)=0$, $t<0$, and $g(t)=1$, $t>LT$. Hence, given h and $f(t)$, for any symbol interval n , the phase $\phi(t, \tilde{\alpha}_n)$ is uniquely defined by the present data symbol α_n , the so-called correlative state vector $(\alpha_{n-1}, \alpha_{n-2}, \dots, \alpha_{n-L+1})$, and the phase state θ_n , where

$$\theta_n = \left[\pi h \sum_{i=-\infty}^{n-L} \alpha_i \right] \text{ modulo } 2\pi \quad (2.7)$$

The number of correlative states is finite and equal to M^{L-1} . For rational modulation indices, let us define the modulation index in terms of integers as

$$h = \frac{2k}{p} \quad k, p = 1, 2, 3, \dots \quad (2.8)$$

There are thus p different phase states with values

$$\theta_n \in \left\{ 0, \frac{2\pi}{p}, \frac{4\pi}{p}, \dots, \frac{(p-1)}{p} 2\pi \right\} \quad (2.9)$$

Thus, the total state of the transmitted signal can

be chosen as the L-tuple

$$\sigma_n = (\theta_n, \alpha_{n-1}, \alpha_{n-2}, \dots, \alpha_{n-L+1}) \quad (2.10)$$

and there are $p M^{(L-1)}$ distinct states. The current data symbol α_n controls the transition from the state σ_n to the next state σ_{n+1} .

It is thus clear that for CPM signaling, the Viterbi algorithm can be used for optimum detection of state sequences and hence, also for detection of the data sequence $\tilde{\alpha}$.

2.2 Convolutionally Encoded CPM

Convolutionally encoded CPM differs from a conventional CPM system by the presence of a convolutional encoder between the source and the modulator. The convolutionally encoded CPM system is given in Figure 2.2.

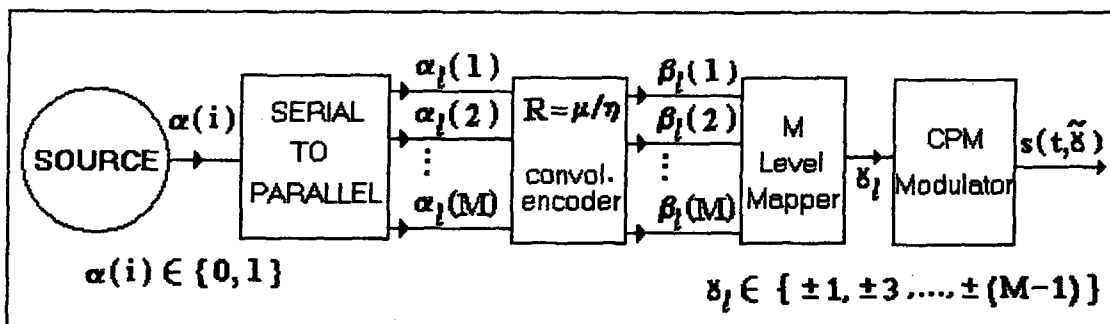


Figure 2.2. Convolutionally Encoded CPM System

The source in Figure 2.2. generates an infinitely long sequence of binary bits 0 and 1, denoted by $\tilde{\alpha} = \dots, \alpha(-1), \alpha(0), \alpha(1), \dots$ at a rate of $1/T_b$ bits/s. Here μ -tuple, $(\alpha_1(1), \alpha_1(2), \dots, \alpha_1(\mu))$, where $\alpha_1(i) = \alpha(1\mu + i - 1)$, enters the rate $R = \frac{\mu}{\eta}$ convolutional encoder. Note that, i is an index for the source generated bits, and l is an index showing the symbol (γ_l) interval. One symbol interval is given by $T = \mu T_b$. As, one block of μ bits, are generated by the source; they enter the serial to parallel converter one by one, and after T seconds, a block of μ bits at the output of the converter, enters the rate $R = \frac{\mu}{\eta}$ convolutional encoder. Note that, for a rate $R = \frac{1}{2}$ convolutional encoder, there is no need for the serial to parallel converter, since $T = T_b$. So, bits generated by the source enters $R = \frac{1}{2}$ convolutional encoder directly. The output of the encoder in Figure 2.2. is the η -tuple $(\beta_1(1), \beta_1(2), \dots, \beta_1(\eta))$. This η -tuple will be mapped into one of the $M = 2^\eta$ channel symbols from the set $\{\pm 1, \pm 3, \dots, \pm(M-1)\}$. Note that, M can also take values that are not equal to 2^η .

Then the coded CPM signal associated with the sequence $\tilde{\gamma} = \dots, \gamma_{-1}, \gamma_0, \gamma_1, \dots$ is

$$S(t, \tilde{\gamma}) = \sqrt{\frac{2E}{T}} \cos(2\pi f_c t + \phi(t, \tilde{\gamma}) + \phi_0) \quad (2.11)$$

where the phase

$$\phi(t, \tilde{\gamma}) = \sum_{i=-\infty}^{\infty} \pi h \gamma_i g(t-iT) \quad (2.12)$$

with $g(t)$ as in (2.3). As μ bits of data are transmitted per symbol interval, $T = \mu T_b$ and $E = \mu E_b$. ϕ_0 is a constant phase shift.

2.2.1 Convolutional Codes

A convolutional code is generated by passing the information sequence to be transmitted through a linear finite-state shift register. In general the shift register consists of v (μ -bit) stages and η linear algebraic function generators. The input data to the encoder, which is assumed to be binary, is shifted into and along the shift register μ bits at a time. The number of output bits, for each μ -bit input sequence, is η bits. So the code rate is defined as $R = \frac{\mu}{\eta}$. The parameter v is called the constraint length of the convolutional code.

Memory is introduced in conventional CPM by means of continuous phase. By convolutionally encoding the generated bits coming from the source, we introduce additional memory to the CPM signal. $\beta_1(m)$ in Figure 2.2 is given by

$$\beta_1(m) = \sum_{i=1}^{\mu} \sum_{j=0} \alpha_{1-j}(i) g_j(i,m) \pmod{2} \quad m=1,2,\dots,\eta \quad (2.13)$$

The binary coefficient $g_j(i,m)$ represents the connection between $\alpha_{1-j}(i)$ and $\beta_1(m)$. It is assumed that, for each i , at least one member of the set $\{g_{v_1}(i,1), \dots, g_{v_1}(i,\eta)\}$ is not equal to zero. The constraint length of the convolutional encoder is then given by $v=v_1+v_2+\dots+v_\mu$.

2.2.2 State Description of Convolutionally Encoded CPM

The correlative state vector for convolutionally encoded CPM can be defined by the state of the encoder at that symbol interval n ; since those bits in the encoder registers effect γ_n .

A coded CPM signal can be regarded as a discrete time Markov process and is best described by a phase tree. A phase tree is the ensemble of phase trajectories for all possible input sequences with a common history at the tree's root node. The vector associated with each node of the phase tree is a possible state of the system and is defined by the vector

$$(\theta_n, \alpha_{n-1}^{(1)}, \dots, \alpha_{n-v_1}^{(1)}, \dots, \alpha_{n-v_\mu}^{(\mu)}) \quad (2.14)$$

where θ_n is the phase

$$\theta_n = \left[\pi h \sum_{i=-\infty}^{n-L} \gamma_i \right] \text{ modulo } 2\pi \quad (2.15)$$

So, $\phi(t, \tilde{\alpha})$ can be uniquely defined by the present data symbol α_n , the correlative state vector given by (2.14), and by θ_n , the phase modulo 2π , at time nT .

2.3 Transmission of CPM

There are several ways to implement CPM modulation. These are phase-locked loop modulators for CPM, CPM modulator with a bandpass filter and hard-limiter, and the basic quadrature transmitter. The basic quadrature transmitter is the most general and the most straightforward way of implementing CPM modulation, so it is stated here. The structure is given in Figure 2.3.

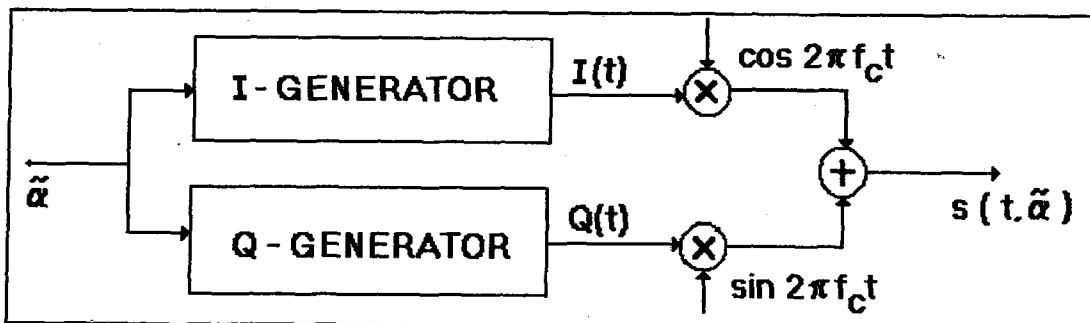


Figure 2.3. Basic Quadrature Transmitter

2.3.1 Basic Quadrature Transmitter

The most straight forward way of implementing a CPM transmitter is to use the basic formula for the modulated signal separated into quadrature components. These are stored in sampled and quantized form in look-up tables, for example, in read only memories (ROMs). The ROM implementation has gained popularity in telephone modem and mobile radio applications.

The normalized transmitter signal $S_o(t, \tilde{\alpha}_n)$ is

$$S_o(t, \tilde{\alpha}_n) = \cos(2\pi f_c t + \phi(t, \tilde{\alpha}_n)) \quad (2.17)$$

where n denotes that we are considering the transmitted signal over the time interval corresponding to the data symbol α_n . The transmitted signal is

$$S(t, \tilde{\alpha}_n) = I(t) \cos(2\pi f_c t) - Q(t) \sin(2\pi f_c t) \quad (2.17)$$

where $\phi(t, \tilde{\alpha}_n)$ is as defined in (2.6) and

$$I(t) = \cos[\phi(t, \tilde{\alpha}_n)] \quad (2.18)$$

$$Q(t) = \sin[\phi(t, \tilde{\alpha}_n)] \quad (2.19)$$

2.4 Receivers for CPM

There are optimum maximum likelihood coherent and noncoherent receivers for CPM. One of them is the optimum Viterbi receiver.

2.4.1 Viterbi Receiver for Conventional CPM

The receiver observes the signal

$$r(t) = S(t, \tilde{\alpha}) + n(t) \quad (2.20)$$

where the noise $n(t)$ is modeled to be Gaussian and white.

The maximum likelihood sequence estimating receiver maximizes the log likelihood function

$$\log_e \left[p_{r(t)|\tilde{\alpha}}(r(t)|\tilde{\alpha}) \right] \approx - \int_{-\infty}^{\infty} [r(t) - S(t, \tilde{\alpha})]^2 dt \quad (2.21)$$

with respect to the infinitely long estimated sequence $\tilde{\alpha}$ (Aulin and Sundberg, 1981a). The maximizing sequence $\tilde{\alpha}$ is the maximum likelihood estimate and $p_{r(t)|\tilde{\alpha}}$ is the probability density function for the observed signal $r(t)$ conditioned on the infinitely long sequence $\tilde{\alpha}$. Maximization of (2.21) is equivalent to the maximization of the correlation

$$J(\tilde{\alpha}) = \int_{-\infty}^{\infty} r(t) S(t, \tilde{\alpha}) dt \quad (2.22)$$

In principle, the operation (2.22) is the basis for a correlation receiver, in which all possible transmitted signals $S(t, \tilde{\alpha})$ are correlated with the received signal and the data sequence $\tilde{\alpha}$ maximizing the correlation is chosen as the received data.

Now define

$$J_n(\tilde{\alpha}) = \int_{-\infty}^{(n+1)T} r(t) S(t, \tilde{\alpha}) dt \quad (2.23)$$

Then

$$J_n(\tilde{\alpha}) = J_{n-1}(\tilde{\alpha}) + Z_n(\tilde{\alpha}) \quad (2.24)$$

where

$$Z_n(\tilde{\alpha}) = \int_{nT}^{(n+1)T} r(t) \cos[\omega_c t + \phi(t, \tilde{\alpha})] dt \quad (2.25)$$

By using the above formulas it is possible to calculate the function $J(\tilde{\alpha})$ recursively through (2.24) and the metric $Z_n(\tilde{\alpha})$. The metric can be recognized as a correlation between the received signal and an estimated signal over the n 'th symbol interval.

The Viterbi algorithm is a recursive procedure to choose those sequences that maximizes the log likelihood

function up to the n 'th symbol interval. The receiver computes $Z_n(\tilde{\alpha}_n, \tilde{\theta}_n)$ for all M^L possible sequences $\{\alpha_{n-1}, \alpha_{n-2}, \dots, \alpha_{n-L+1}\}$ and all p possible $\tilde{\theta}_n$. This makes pM^L different values of Z_n .

2.5 Error Performance

When the CPM signal is assumed to be transmitted over an additive, white, Gaussian noise channel having one-sided noise power spectral density N_0 W/Hz; the exact error performance of coded and uncoded CPM signal is difficult to evaluate. However, for large signal to noise ratio (given as E_b/N_0), the symbol error probability will approach to the lower bound

$$P_e \approx C Q \left[\sqrt{d_{\min}^2 E_b / N_0} \right] \quad (2.26)$$

where C is a constant independent of E_b/N_0 and $Q(x)$ is the area under the unit variance normal curve from x to ∞ , (Lindell et al, 1986)

$$Q(x) = \frac{1}{\sqrt{2\pi}} \int_x^{\infty} e^{-t^2/2} dt \quad (2.27)$$

The term d_{\min}^2 is the minimum normalized squared Euclidean distance (MNSED) of the coded signal, defined as

$$d_{\min}^2 = \min \frac{1}{2E_b} \int_0^{\infty} [S(t, \gamma) - S(t, \tilde{\gamma})]^2 dt \quad (2.28)$$

where $S(t, \gamma)$ and $S(t, \tilde{\gamma})$ are two possible transmitted signals corresponding to the sequences $\{\gamma\}$ and $\{\tilde{\gamma}\}$. Let $E_c(\cdot)$ denote the encoding/mapping operation in Figure 2.2. which transforms $\tilde{\alpha} = \dots, \dots, \alpha_{-1}, \alpha_0, \alpha_1, \dots$ into $\tilde{\gamma} = \dots, \gamma_{-1}, \gamma_0, \gamma_1, \dots$. The minimization in (2.28) is over all those pairs of sequences $\tilde{\gamma} = E_c(\tilde{\alpha})$ and $\tilde{\gamma}' = E_c(\tilde{\alpha}')$ with $(\alpha(0), \dots, \alpha(\mu)) \neq (\alpha'(0), \dots, \alpha'(\mu))$ and $\alpha(k) = \alpha'(k)$ for $k < 0$. It is clear from (2.26) that at large E_b/N_0 , the power efficiency of a modulation scheme is determined by its MNSED.

CHAPTER III

UNCODED AND ENCODED CPFSK SCHEMES

3.1 Introduction

In this chapter, how the uncoded and convolutionally encoded CPM systems are simulated for the AWGN channel is presented. Also, because of its importance the calculation of the minimum normalized squared Euclidean distance (MNSD) is given in the following section.

3.2 MINIMUM NORMALIZED SQUARED EUCLIDEAN DISTANCE

As it is seen from (2.26), MNSD is of great importance for CPM signals. As we have larger MNSD, we get better error performance. So, convolutional encoding is used in conjunction with CPM to achieve larger MNSD. For the convolutionally encoded CPM system sketched in Figure 2.2., with the constraint length v for the convolutional encoder; the best MNSD achievable has to be found through an exhaustive search over all possible

combinations of convolutional codes and mapping rules; as it is seen from (2.28). It must be noted that, even if the code and the mapping rule is given; it isn't easy to find the two sequences that begin with the same state at a given time and split from that point and remerge at some later time; say after interval length of NT .

At the remerge point the states of the two sequences; $(\theta_k, \alpha_{k-1}(1), \dots, \alpha_{k-V}(\mu))$ and $(\theta'_k, \alpha'_{k-1}(1), \dots, \alpha'_{k-V}(\mu))$ must be the same. This is required because, after the remerge point the phases of two sequences must be the same for a given input α_{k+1} .

To calculate the MNSSED for an observation length of N symbols, all pairs of phase trajectories in the phase tree over N symbol intervals must be considered. The Euclidean distance is calculated according to (2.28) for all these pairs, and the minimum of these Euclidean distances is the desired result. Note that, for pairs of sequences, called 1 and 2, that split and remerge after a time of length NT ; we define the distance measure

$$d_{12}^2(N) = \frac{1}{2E_b} \int_0^{NT} [S(t, \tilde{\gamma}) - S(t, \tilde{\gamma}')]^2 dt \quad (3.1)$$

It is clear that, for a fixed pair of phase trajectories, the Euclidean distance is a nondecreasing function of the observation length N .

For $W_c \gg \frac{2\pi}{T}$, equation (3.1) reduces to

$$d_{12}^2(N) \approx \frac{1}{T} \int_0^{NT} [1 - \cos(\Delta\phi(t))] dt \quad (3.2)$$

where $\Delta\phi(t) = \phi(t, \tilde{\gamma}) - \phi(t, \tilde{\gamma}')$, is the time varying phase separation between the two signals of length NT (Mulligan and Wilson, 1984).

Observe that, MNSD depends on h , the modulation index; $\phi(t, \tilde{\gamma})$, the phase modulation characteristic; and the memory of the encoding process. Note that, the cumulative squared distance may be recursively computed as

$$d_{12}^2(N+1) = d_{12}^2(N) + \frac{1}{T} \int_{NT}^{(N+1)T} [1 - \cos(\Delta\phi(t))] dt \quad (3.3)$$

(Mulligan and Wilson, 1984).

Now, we are going to examine MNSD on an example. The system is as in Figure 2.2.. We have $h=3/10$, rate $R=1/2$ convolutionally encoded four level CPFSK with natural mapping. The two code generator polynomials of the code are given by $G_1(D)=1+D+D^2$ and $G_2(D)=D$. The octal representation of $G_1(D)$ is 7 and the octal representation of $G_2(D)$ is 2. So, the octal representation of this code is given by (7,2).

Since we have CPFSK, $f(t)$ is given by

$$f(t) = \begin{cases} \frac{1}{T} & , 0 \leq t \leq T \\ 0 & , \text{elsewhere} \end{cases}$$

In Figure 3.1., we have the rate $R=1/2$, $(7,2)$ convolutional encoder and four level mapper. The adder is a modulo 2 adder.

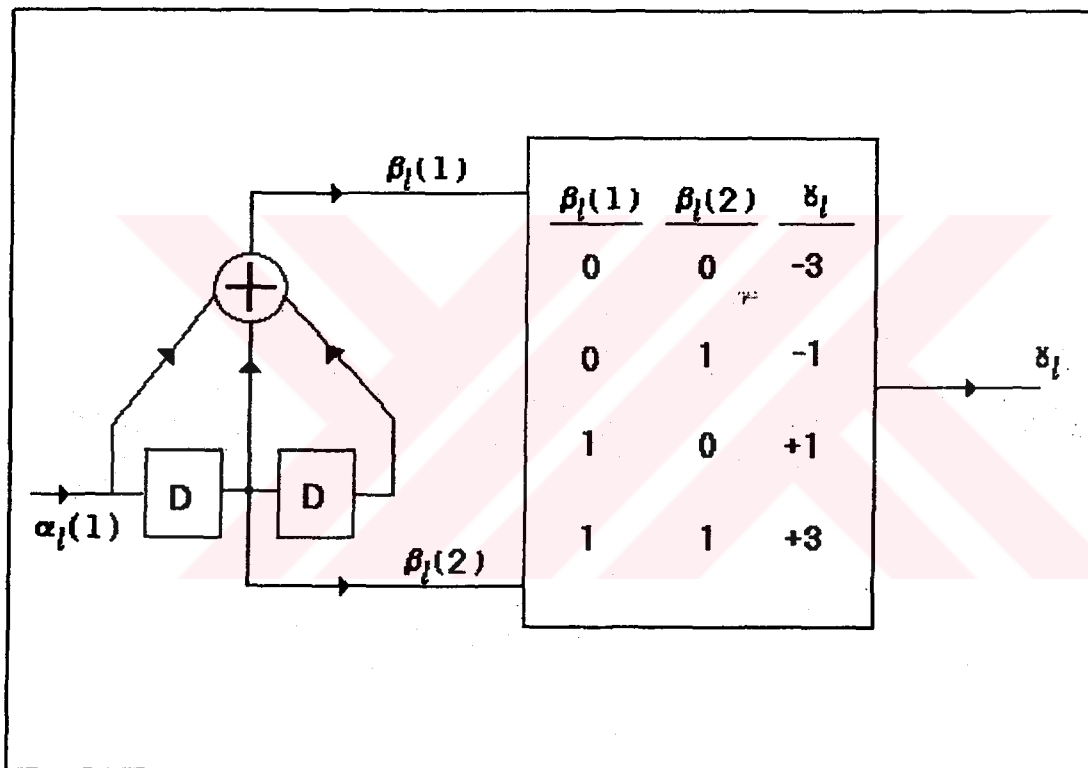


Figure 3.1. Rate 1/2 (7,2) Convolutional Encoder and Four-Level Mapper.

The corresponding phase tree when combined with CPFSK, is given in Figure 3.2.

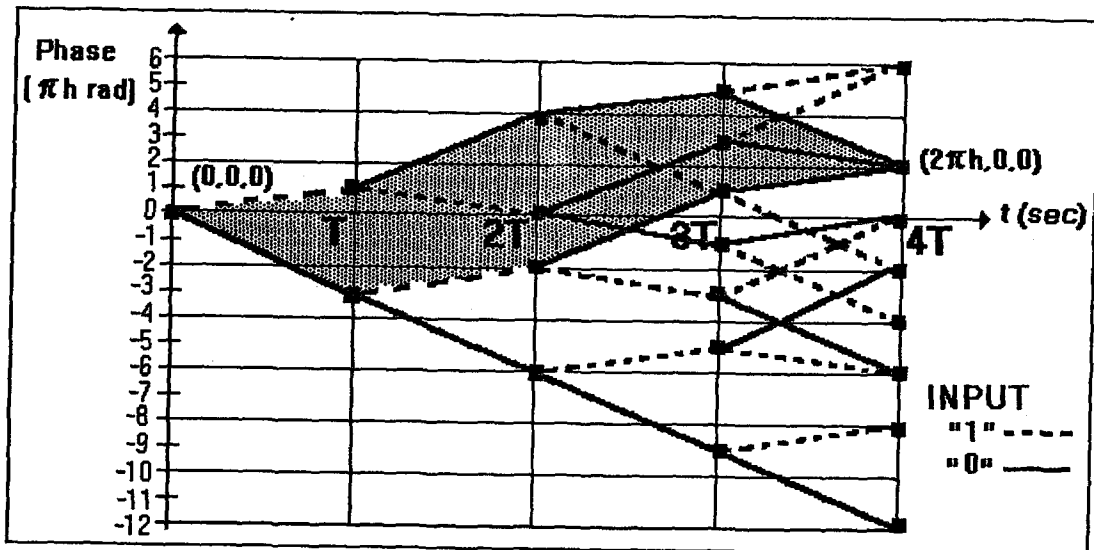


Figure 3.2. Corresponding Phase Tree When Rate 1/2 Convolutional Encoder and Four-Level Mapper Combined with CPFSK.

In Figure 3.2., the two paths forming the boundary of the shaded area, merge at state $(2\pi h, 0, 0)$, four intervals after the initial state splits at state $(0, 0, 0)$. It can be shown that, for this system no other merge can occur before time $4T$. The merge at point $3T$ is not an actual merge point because, at the merge point in $3T$ the states of the two paths are not the same, since $\alpha_{k-1}, \alpha_{k-2}$ are different for them. They are $(1, 0)$ and $(0, 0)$ which are not the same. So they will go to a different state for a given source input α_k . Thus, unlike uncoded CPFSK where a merge can occur in two symbol intervals, the minimum merge length is increased by prior encoding of the data symbols. Generally, the longer the

merge length, the larger the MNSED and hence, the better the error performance.

Now, we will find MNSED for the system given in Figure 3.1.. For the two paths forming the boundary of the shaded area in Figure 3.2. we have the equation (3.2) where $N=4$, and

$$\begin{aligned}
 d_{12}^2(1) &= \frac{1}{T} \int_0^T [1 - \cos(\frac{t}{T} \pi h (\gamma_0 - \gamma'_0))] dt \\
 &= \frac{1}{T} \int_0^T [1 - \cos(\frac{t}{T} \frac{3\pi}{10} 4)] dt \\
 &= 1.15591.
 \end{aligned}$$

$d_{12}^2(2)$, $d_{12}^2(3)$, $d_{12}^2(4)$ are found to be 2.15591, 3.15591 and 4.31182 respectively, after some calculations.

For these two paths we have $d_{\min}^2 = d_{12}^2(4)$. So, no other two paths can be found to give a smaller normalized distance (Ho and Mclane, 1988).

As the modulation index h is changed, the paths giving MNSED and the value of MNSED are changing. For example, for the same encoder given in Figure 3.1. for $h=1/4$; the two paths giving MNSED is not the same as the two paths forming the boundary of the shaded area in

Figure 3.2.. We found $d_{12}^2(4)$, for $h=1/4$ for these two paths forming the boundary of the shaded area in Figure 3.2.; $d_{12}^2(1)$, $d_{12}^2(2)$, $d_{12}^2(3)$, $d_{12}^2(4)$ are found to be 1, 2.636, 4.2732 and 5.273 respectively. But MNSSED is equal to 4.30 for another pair of paths (Ho and McLane, 1988). Also N_{dmin} , MNSSED event length is equal to 6.

For $h=1/6$, for the same code and 4-Level CPFSK scheme; we have found $d_{12}^2(1)$, $d_{12}^2(2)$, $d_{12}^2(3)$, $d_{12}^2(4)$ as 0.586, 2, 3.826 and 3.4125 respectively, for the two paths forming the boundary of the shaded area in Figure 3.2.. But MNSSED is equal to 2.42, for MNSSED event length of N_{dmin} equal to 6 (Ho and McLane, 1988). More details of $d_{12}^2(4)$ calculations for $h=3/10$, $h=1/6$ and $h=1/4$ are given in Appendix A.

So, as it is seen from the example; for different values of h , MNSSED and the sequences of minimum distance event; in other words, minimum distance event length, are different. So, to find MNSSED, every pair of sequences that split and remerge must be considered. This is an exhaustive work and several algorithms are developed to find MNSSED (Mulligan and Wilson, 1984).

For the encoded 4-level CPFSK example MNSSED and minimum distance event length are given in Table 3.1..Note that MNSSED increases as h increases.

Table 3.1 MNSSED and Minimum Distance Event Length Table
for (7,2) Coded CPFSK.

h	d_{\min}^2	code	N_{\min}
1/6	2.42	(7,2)	6
1/4	4.30	(7,2)	6
3/10	4.31	(7,2)	4

As it is seen from Table 3.1. and from our calculations, the paths forming the MNSSED event do not correspond to the shortest length paths that split and remerge as soon as possible. In the example, this is the case for the two paths forming the boundary of the shaded area. These paths are the shortest length paths that split and remerge as soon as possible. But for $h=1/6$ and for $h=1/4$, two longer paths of length 6 give the minimum distance event.

3.3 The Effect of Channel Noise

The simulation of a CPM system may be broken into parts. First of all, we must simulate the effect of channel noise. Second, we must construct a receiver and then analyze the error performance of the receiver. In this section the simulation of noise is introduced. A general CPM system with AWGN and Viterbi receiver is given in Figure 3.3.

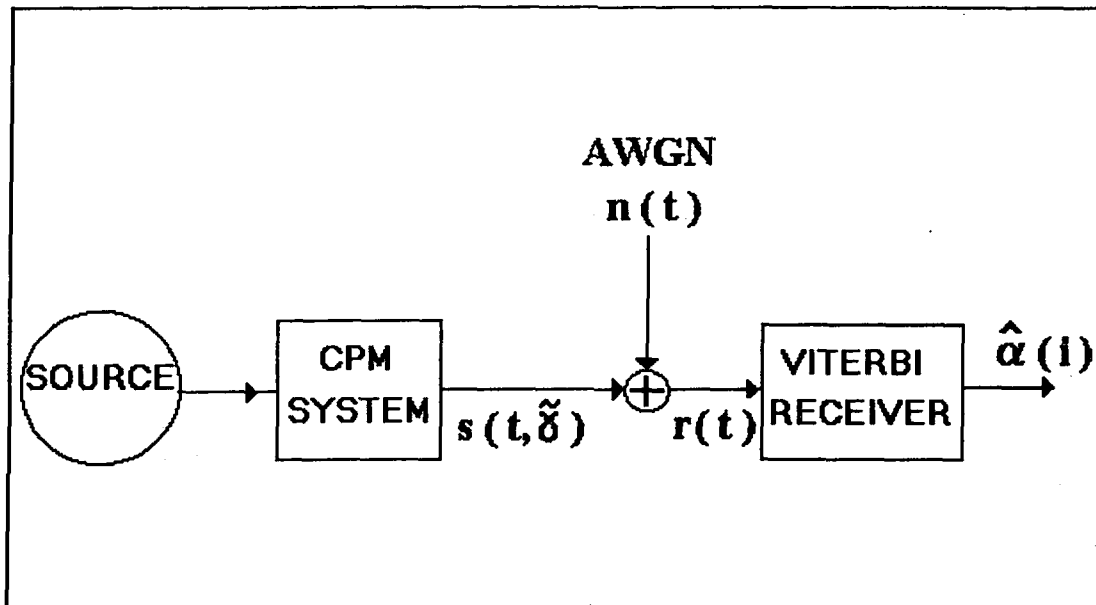


Figure 3.3. General CPM System with AWGN and with Viterbi Receiver

CPM system in the figure is an uncoded or convolutionally encoded CPM system. One procedure to simulate channel noise, in common use, is to form a discrete-time approximation to the modulated signal. The signal is sampled each $\frac{T}{\epsilon}$ second, or ϵ times at each interval of length T , and the assumption is made that the signal holds that sample value throughout the $\frac{T}{\epsilon}$ second subinterval. During the subinterval, $s(t)$ holds a constant value; and for each subinterval an uncorrelated Gaussian variable is added to the signal at that subinterval. The proper number of points is best found experimentally by increasing the point count until no change in the results occur (Anderson et al, 1986:258).

Another method of simulating channel noise is the so-called signal space method. And we have used this method to simulate AWGN of the channel, for all our uncoded and coded CPFSK systems.

3.3.1 Signal Space Method

To simulate the effect of an AWGN channel on a decoder, we express the signals in terms of components along the orthogonal directions of a signal space, the so-called signal space method. We perform a Gram-Schmidt orthogonalization procedure on the phase signals to produce a basis for the vector space of transmitted signals. The channel adds Gaussian noise of power $\frac{N_0}{2}$ to each component, and the decoder finds the closest signal to this received vector in Euclidean distance.

One fact about the signal space method is; you must produce an orthogonal basis with proper dimensions for the used CPM system. The advantage of this method is that, the simulation takes less time than the discrete-time approximation given in section 3.3, since we do not need to compute metrics for the Viterbi decoder by taking integrals for every symbol interval.

3.4 Uncoded CPFSK

In this section, simulation of the uncoded CPFSK is presented. The orthonormal functions and vector representation of the modulated signals are given and, introduction of the AWGN to the channel, by the signal space method for CPFSK system is explained. A coherent Viterbi receiver is introduced to decode the incoming bits from the source.

The system is as in Figure 2.1., with the source generating bits ± 1 , randomly. We have the CPFSK signal as

$$S(t, \tilde{\alpha}_n) = \sqrt{\frac{2E}{T}} \cos\left(\omega_c t + \alpha_n \pi h \frac{(t-nT)}{T} + \theta_n\right) \quad (3.4.a)$$

$nT \leq t \leq (n+1)T$

where θ_n is the phase at the start of the symbol interval,

ω_c is the radian carrier frequency,

h is the modulation index,

α_n is the symbol sent in the n 'th interval,

T is the symbol interval time,

E is the symbol energy.

Using some trigonometric identities, the signal can be re-written as

$$\begin{aligned}
S(t, \tilde{\alpha}_n) &= \sqrt{\frac{2E}{T}} \cos\left(\omega_c t + \alpha_n \pi h \frac{(t-nT)}{T}\right) \cos \theta_n \\
&- \sqrt{\frac{2E}{T}} \sin\left(\omega_c t + \alpha_n \pi h \frac{(t-nT)}{T}\right) \sin \theta_n \quad (3.4.b) \\
&\quad nT \leq t \leq (n+1)T
\end{aligned}$$

The number of modulation signals is twice the number of α_n . For binary CPFSK we have $\alpha_n \in \{\pm 1\}$ and thus the modulation signals are:

$$S_1(t) = \sqrt{\frac{2}{T}} \cos\left(\omega_c t + \frac{\pi h t}{T}\right)$$

$$S_2(t) = \sqrt{\frac{2}{T}} \sin\left(\omega_c t + \frac{\pi h t}{T}\right)$$

$$S_3(t) = \sqrt{\frac{2}{T}} \cos\left(\omega_c t - \frac{\pi h t}{T}\right)$$

$$S_4(t) = \sqrt{\frac{2}{T}} \sin\left(\omega_c t - \frac{\pi h t}{T}\right)$$

where $0 \leq t \leq T$.

So, four signal dimensions are required during each symbol interval to represent the 2-level CPFSK. To express the modulation signals in vector form on an orthonormal basis, we apply the Gram-schmidt procedure to the 4 modulation signals and we have created a 4 dimensional orthonormal basis for 2-level CPFSK. The

derivation of the basis is given in Appendix B. The basis functions are:

$$\Phi_1(t) = \sqrt{\frac{2}{T}} \cos\left(\omega_c t + \frac{\pi h t}{T}\right) \quad (3.5.a)$$

$$\Phi_2(t) = \sqrt{\frac{2}{T}} \sin\left(\omega_c t + \frac{\pi h t}{T}\right) \quad (3.5.b)$$

$$\Phi_3(t) = \frac{S_3(t) - S_o \Phi_1(t) - C_o \Phi_2(t)}{D_1} \quad (3.5.c)$$

$$\Phi_4(t) = \frac{S_4(t) + C_o \Phi_1(t) - S_o \Phi_2(t)}{D_1} \quad (3.5.d)$$

where

$$S_o = \frac{\sin(2\pi h)}{2\pi h}, \quad C_o = \frac{1 - \cos(2\pi h)}{2\pi h}, \quad D_1 = (1 - S_o^2 - C_o^2)^{1/2}$$

The signal in the n'th baud interval can be expressed in terms of the basis vectors as

$$S(t, \tilde{\alpha}_n) = \sqrt{E} \sum_{i=1}^4 A_{ni} \Phi_i(t) \quad (3.6)$$

where α_{ni} is the coefficient corresponding to $\Phi_i(t)$ during this interval. The coefficients for the signal vectors obtained by expressing $S(t, \tilde{\alpha}_n)$ in terms of the modulation signals from equation (3.4.b) and then expressing the $S_n(t)$ in terms of $\Phi_i(t)$ are given in Table 3.2, where S_o , C_o , D_1 are defined above and θ_n is the phase at the beginning of the symbol interval.

Table 3.2 Coefficients for the Signal Vectors
for Uncoded 2 Level CPFSK

	+1	-1
A_{n1}	$\cos\theta_n$	$S_o \cos\theta_n + C_o \sin\theta_n$
A_{n2}	$-\sin\theta_n$	$C_o \sin\theta_n - S_o \cos\theta_n$
A_{n3}	0	$D_1 \cos\theta_n$
A_{n4}	0	$-D_1 \sin\theta_n$

Similarly, white Gaussian noise having a two-sided power spectral density can be projected on this signal space and expressed as

$$n_i(t) = \sum_{i=1}^4 n_i \Phi_i(t) \quad (3.7)$$

where n_i , $i=1,2,3,4$ are independent identically distributed Gaussian random variables with zero mean and a variance of $\frac{N_o}{2}$.

Now, as we add the AWGN components to each signal space vector component forming $s(t)$, we get the projection of the received signal $r(t)$ as

$$r(t) = \sqrt{E} \sum_{i=1}^4 A_{ni} \Phi_i(t) + \sum_{i=1}^4 n_i \Phi_i(t)$$

and after re-arranging the terms, we have

$$r(t) = \sum_{i=1}^4 B_{ni} \Phi_i(t) \quad (3.8)$$

where

$$B_{ni} = \sqrt{E} A_{ni} + n_i .$$

3.4.1 The Viterbi Algorithm and the Simulation

We have discussed the Viterbi algorithm in section 2.4.1 and have the metric $Z_n(\tilde{\alpha})$ as in (2.25); now as we insert $r(t)$ of equation (3.8) and $S(t, \tilde{\alpha})$ of equation (3.6) into this metric equation we have

$$Z_n(\tilde{\alpha}) = \int_{nT}^{(n+1)T} \left[\sqrt{E} \sum_{i=1}^4 A_{ni} \Phi_i(t) \right] \left[\sum_{j=1}^4 B_{nj} \Phi_j(t) \right] dt$$

using the fact that $\Phi_1, \Phi_2, \Phi_3, \Phi_4$ are the vectors of an orthonormal basis we have

$$Z_n(\tilde{\alpha}) = \sqrt{E} \sum_{i=1}^4 A_{ni} B_{ni} \quad (3.9)$$

The Viterbi algorithm is a recursive procedure to choose those sequences that maximize the log likelihood function up to the n 'th symbol interval. The receiver computes $Z_n(\alpha_n, \theta_n)$ for all possible α_n and p possible θ_n . This makes $2p$ different values of Z_n . Remember that the state description of the uncoded CPM was given in section 2.1.

We have made the simulation for binary CPFSK, for the modulation indices $h=1/2$ and $h=1/4$. The state trellis diagram for $h=1/2$, $h=1/4$ are given in Figure 3.4. and Figure 3.5. respectively. Also, all transmitted signal space vectors for $h=1/2$, $h=1/4$ are given in Table 3.3. and Table 3.4. respectively.

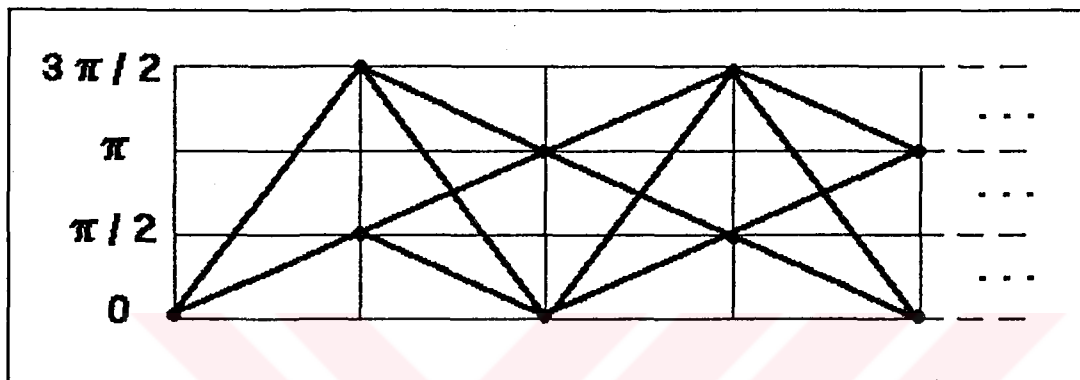


Figure 3.4. The State Trellis Diagram for $h=1/2$ Uncoded CPFSK

Table 3.3 All Transmitted Signal Space Vectors for $h=1/2$ Uncoded CPFSK

Initial Phase	Phase Slope	Signal Space Vector Components			
		A_{n1}	A_{n2}	A_{n3}	A_{n4}
0	0.5	1	0	0	0
$\pi/2$	0.5	0	-1	0	0
π	0.5	-1	0	0	0
$3\pi/2$	0.5	0	1	0	0
0	-0.5	0	C_0	D_1	0
$\pi/2$	-0.5	C_0	0	0	$-D_1$
π	-0.5	0	$-C_0$	$-D_1$	0
$3\pi/2$	-0.5	$-C_0$	0	0	D_1

Table 3.4 All Transmitted Signal Space Vectors for $h=1/4$
Uncoded CPFSK.

Initial Phase	Phase Slope	Signal A_{n1}	Space Vector A_{n2}	Vector A_{n3}	Components A_{n4}
0	0.25	1	0	0	0
$\pi/4$	0.25	.707	-.707	0	0
$\pi/2$	0.25	0	-1	0	0
$3\pi/4$	0.25	-.707	-.707	0	0
π	0.25	-1	0	0	0
$5\pi/4$	0.25	-.707	.707	0	0
$3\pi/2$	0.25	0	1	0	0
$7\pi/4$	0.25	.707	-.707	0	0
0	-0.25	.637	.637	.435	0
$\pi/4$	-0.25	.9	0	.300	-.300
$\pi/2$	-0.25	.637	-.637	0	-.435
$3\pi/4$	-0.25	0	-.900	-.300	-.300
π	-0.25	-.637	-.637	-.435	0
$5\pi/4$	-0.25	-.900	0	-.300	.300
$3\pi/2$	-0.25	-.637	.637	0	.435
$7\pi/4$	-0.25	0	.900	.300	.300

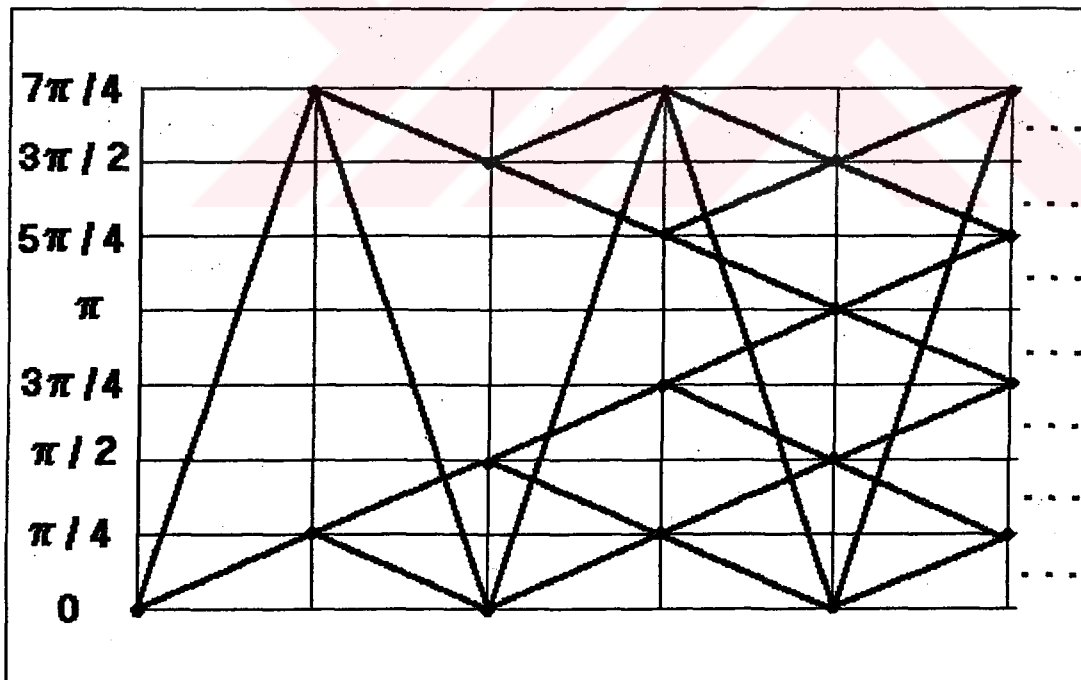


Figure 3.5. The State Trellis Diagram for $h=1/4$ Uncoded CPFSK

So, as it is seen from Figures 3.4. and 3.5., we have 4 possible states for $h=1/2$ case, and 8 possible states for $h=1/4$ case. The Viterbi algorithm assumes that; all possible transmitted finite sequences start from the state 1, corresponding to zero phase, and end in the same state.

The Viterbi algorithm calculates 4 metrics for $h=1/2$ and 8 metrics for $h=1/4$, for each symbol interval. We assume that all metrics are zero initially. Then the metrics for each state are computed and updated recursively. There are two possible paths entering each state, and the path with the smallest metric is deleted. The undeleted one is called the survivor. At each state in the trellis, the surviving paths are saved only back to a certain point, a length called the path memory N_T . At this delay a decision on the first symbol is forced by choosing the largest metric path's first symbol. Then at N_{T+1} we decide on the second symbol by the same way, and this goes on. By making a decision after N_T symbol intervals, we have relied on the fact that, a path which has splitted from the correct path will accumulate distance from it in proportion to the length of the unmerged span. Incorrect paths will have a low probability of having a long unmerged span.

We have taken the path memory N_T to be 50 channel symbol intervals, for all our simulations, which is large enough to ensure that all unmerged pairs have a distance greater than MNSD (Lindell et al, 1988).

We have used a table to store the state transitions caused by each data symbol from each state, and another table which stores the backwards state information, the states from which it is possible to enter each state. The transmitter uses the first table and the receiver the second. For each state; a memory is maintained to store the metric of the best path leading into the state at the present time, the identity of the path, that is the data symbols corresponding to it, and certain temporary information.

Considering the whole simulation; we generate random binary bits, we modulate them and obtain signal space vectors for each corresponding bit, that are given in Table 3.3. and Table 3.4.. Then, we add an independent, identically distributed Gaussian variate of variance $\frac{N_0}{2}$ on to each component to form the components of the received noisy signal (Press et al, 1988). Then beginning with the first state initially, the algorithm seeks the best metric path leading into each state at the next time. There are 2 paths out of each state at the present time and into each state at the next time. So, two

metrics, for each state in that interval, is calculated. The path giving the smallest metric is deleted. And after the path memory length is reached, we begin to decide on transmitted symbols one by one as the algorithm goes on, in the same manner.

And, we measure the error performance of the receiver by comparing the output symbols with the known transmitted symbols.

3.5 Simulation of the Convolutionally Encoded CPFSK with $R=1/2$, (7,2) Code

In our work, we have used $R=1/2$, (7,2) convolutional code, given with the four level mapping in section 3.1; and CPFSK signalling scheme is also used for this part of the work. We have chosen the (7,2) convolutional code because of its good performance; that is it has large MNSD (Lindell et al,1988), (Ho and McLane,1988). Note that, $R=2/3$ convolutional codes and $R=1/2$ convolutional codes are the most popular convolutional codes, used with CPM in literature.

In the following subsections, first the orthonormal functions and vector representation of the modulated signals are given; and the introduction of AWGN to the

system by the signal space method is presented. Next, the modifications for the Viterbi algorithm of the convolutionally encoded CPFSK for $h=1/4$ is stated and then, the simulation system is explained.

3.5.1 Orthonormal Functions and Vector Representation of the Transmitted Signals

The convolutionally encoded CPM system was given in Figure 2.2.. Since rate $R=1/2$ convolutional encoder is used; as indicated before, we do not need the serial to parallel converter. The $R=1/2$, $(7,2)$ convolutional encoder with 4-level mapper, that was given in detail in Figure 3.1., is used. The source generates bits 1 and 0 randomly. We have $\mu=1$ and $\eta=2$, so we have 4-ary signalling. That is $\tilde{\gamma}_n$ takes values $\{\pm 1, \pm 3\}$ at the n 'th symbol interval. For the CPFSK signalling scheme, we have the CPFSK signal at the output of the 4-level mapper as:

$$S(t, \tilde{\gamma}) = \sqrt{\frac{2E}{T}} \cos\left(Wc t + \gamma_n \pi h \frac{(t-nT)}{T} + \theta_n \right) \quad (3.10.a)$$

$$nT \leq t \leq (n+1)T$$

Note that, α_n is the generated bit by the random generator at the n 'th symbol interval, but γ_n is the output bit of the 4-level mapper. θ_n, Wc, h, T and E are as given in section 2. The relation between $\alpha_n, \alpha_{n-1}, \alpha_{n-2}$ and γ_n is given in Table 3.5.

Table 3.5 The Relation Between the Generated bits and the Output Bit of the 4-Level Mapper.

α_n	α_{n-1}	α_{n-2}	γ_n
0	0	0	-3
0	0	1	+1
0	1	0	+3
0	1	1	-1
1	0	0	+1
1	0	1	-3
1	1	0	-1
1	1	1	+3

Using basic trigonometric identities, the signal in equation (3.10.b) can be re-written as:

$$\begin{aligned}
 S(t, \tilde{\gamma}_n) = & \sqrt{\frac{2E}{T}} \cos\left(\omega_c t + \gamma_n \pi h \frac{(t-nT)}{T}\right) \cos \theta_n \\
 & - \sqrt{\frac{2E}{T}} \sin\left(\omega_c t + \gamma_n \pi h \frac{(t-nT)}{T}\right) \sin \theta_n \quad (3.10.b)
 \end{aligned}$$

$nT \leq t \leq (n+1)T$

The number of modulation signals is twice the number of γ_i . Since γ_i can take the values $\{\pm 1, \pm 3\}$, we have the modulation signals as:

$$S_1(t) = \sqrt{\frac{2E}{T}} \cos\left(\omega_c t + \frac{\pi h t}{T}\right)$$

$$S_2(t) = \sqrt{\frac{2E}{T}} \sin\left(\omega_c t + \frac{\pi h t}{T}\right)$$

$$S_3(t) = \sqrt{\frac{2E}{T}} \cos\left(\omega_c t - \frac{\pi h t}{T}\right)$$

$$S_4(t) = \sqrt{\frac{2}{T}} \sin\left(\omega_c t - \frac{\pi h t}{T}\right)$$

$$S_5(t) = \sqrt{\frac{2}{T}} \cos\left(\omega_c t + \frac{3\pi h t}{T}\right)$$

$$S_6(t) = \sqrt{\frac{2}{T}} \sin\left(\omega_c t + \frac{3\pi h t}{T}\right)$$

$$S_7(t) = \sqrt{\frac{2}{T}} \cos\left(\omega_c t - \frac{3\pi h t}{T}\right)$$

$$S_8(t) = \sqrt{\frac{2}{T}} \sin\left(\omega_c t - \frac{3\pi h t}{T}\right)$$

where $0 \leq t \leq T$.

So, eight signal dimensions are required during each symbol interval to represent the 4-Level CPFSK signal obtained with $R=1/2$ convolutional encoder. To express the modulation signals in vector form on an orthonormal basis, we have applied the Gram-Schmidt procedure to the 8 modulation signals and we have created an 8 dimensional orthonormal basis for 4-Level convolutionally encoded CPFSK. The derivation of the basis is given in Appendix B. The basis functions are:

$$\Phi_1(t) = \sqrt{\frac{2}{T}} \cos\left(\omega_c t + \frac{\pi h t}{T}\right) \quad (3.11.a)$$

$$\Phi_2(t) = \sqrt{\frac{2}{T}} \sin\left(\omega c t + \frac{\pi h t}{T}\right) \quad (3.11.b)$$

$$\Phi_3(t) = \frac{S_3(t) - S_0 \Phi_1(t) - C_0 \Phi_2(t)}{D_1} \quad (3.11.c)$$

$$\Phi_4(t) = \frac{S_4(t) + C_0 \Phi_1(t) - S_0 \Phi_2(t)}{D_1} \quad (3.11.d)$$

$$\Phi_5(t) = \frac{S_5(t) - S_0 \Phi_1(t) + C_0 \Phi_2(t) - b_{53} \Phi_3(t) - b_{54} \Phi_4(t)}{D_2} \quad (3.11.e)$$

$$\Phi_6(t) = \frac{S_6(t) - C_0 \Phi_1(t) - S_0 \Phi_2(t) + b_{54} \Phi_3(t) - b_{53} \Phi_4(t)}{D_2} \quad (3.11.f)$$

$$\Phi_7(t) = \frac{1}{D_3} \left[S_7(t) - S_1 \Phi_1(t) - C_1 \Phi_2(t) - b_{73} \Phi_3(t) - b_{74} \Phi_4(t) \right. \\ \left. - b_{75} \Phi_5(t) - b_{76} \Phi_6(t) \right] \quad (3.11.g)$$

$$\Phi_8(t) = \frac{1}{D_3} \left[S_8(t) + C_1 \Phi_1(t) - S_1 \Phi_2(t) + b_{74} \Phi_3(t) - b_{73} \Phi_4(t) \right. \\ \left. + b_{76} \Phi_5(t) - b_{75} \Phi_6(t) \right] \quad (3.11.h)$$

where

$$S_0 = \frac{\sin(2\pi h)}{2\pi h}, \quad C_0 = \frac{1 - \cos(2\pi h)}{2\pi h},$$

$$S_1 = \frac{\sin(4\pi h)}{4\pi h}, \quad C_1 = \frac{1 - \cos(4\pi h)}{4\pi h},$$

$$b_{53} = \frac{S_1 - S_0^2 + C_0^2}{D_1}, \quad b_{54} = \frac{2C_0 S_0 - C_1}{D_1},$$

$$b_{73} = \frac{S_0 - S_0 S_1 - C_0 C_1}{D_1}, \quad b_{74} = \frac{C_0 + C_0 S_1 - S_0 C_1}{D_1},$$

$$b_{75} = \frac{S_2 - S_0 S_1 + C_0 C_1 - b_{53} b_{73} - b_{54} b_{74}}{D_2},$$

$$b_{76} = \frac{C_2 - C_0 S_1 - S_0 C_1 + b_{54} b_{73} - b_{53} b_{74}}{D_2},$$

$$S_2 = \frac{\sin(6\pi h)}{6\pi h}, \quad C_2 = \frac{1 - \cos(6\pi h)}{6\pi h},$$

$$D_1 = (1 - S_0^2 - C_0^2)^{1/2}, \quad D_2 = (1 - S_0^2 - C_0^2 - b_{53}^2 - b_{54}^2)^{1/2}.$$

$$D_3 = (1 - S_1^2 - C_1^2 - b_{73}^2 - b_{74}^2 - b_{75}^2 - b_{76}^2)^{1/2}.$$

Similar to the uncoded CPFSK, the signal in the n'th baud interval can be expressed in terms of the basis vectors as

$$S(t, \tilde{\gamma}_n) = \sqrt{E} \sum_{i=1}^B A_{ni} \Phi_i(t) \quad (3.12)$$

where A_{ni} is the coefficient corresponding to $\Phi_i(t)$ during this interval. The coefficients for the transmitted signal vectors, obtained by expressing $S(t, \tilde{\gamma}_n)$ in terms of the modulation signals from (3.10.b) and then expressing $S_n(t)$ in terms of $\Phi_i(t)$, are given in Table 3.6. where $S_0, C_0, D_1, D_2, D_3, S_1, C_1, b_{53}, b_{54}, b_{73}, b_{74}, b_{75}$ and b_{76} are defined above and θ_n is the phase at the beginning of the symbol interval.

Table 3.6 Coefficients for the Transmitted Signal Vectors for R=1/2 (7,2) Convolutionally Encoded CPFSK.

	+1	-1	+3	-3
A_{i1}	$\cos\theta_n$	$S_0 \cos\theta_n$ $+C_0 \sin\theta_n$	$S_0 \cos\theta_n$ $-C_0 \sin\theta_n$	$S_0 \cos\theta_n$ $+C_0 \sin\theta_n$
A_{i2}	$-\sin\theta_n$	$C_0 \cos\theta_n$ $-S_0 \sin\theta_n$	$-C_0 \cos\theta_n$ $-S_0 \sin\theta_n$	$C_0 \cos\theta_n$ $-S_0 \sin\theta_n$
A_{i3}	0	$D_1 \cos\theta_n$	$b_{53} \cos\theta_n$ $+b_{54} \sin\theta_n$	$b_{73} \cos\theta_n$ $+b_{74} \sin\theta_n$
A_{i4}	0	$-D_1 \sin\theta_n$	$b_{54} \cos\theta_n$ $-b_{53} \sin\theta_n$	$b_{74} \cos\theta_n$ $-b_{73} \sin\theta_n$
A_{i5}	0	0	$D_2 \cos\theta_n$	$b_{75} \cos\theta_n$ $+b_{76} \sin\theta_n$
A_{i6}	0	0	$-D_2 \sin\theta_n$	$b_{76} \cos\theta_n$ $-b_{75} \sin\theta_n$
A_{i7}	0	0	0	$D_3 \cos\theta_n$
A_{i8}	0	0	0	$-D_3 \sin\theta_n$

Similar to the uncoded case, white Gaussian noise with two-sided power spectral density, can be projected on this 8 dimensional signal space and expressed as

$$n_i(t) = \sum_{i=1}^8 n_i \phi_i(t) \quad (3.13)$$

where n_i , $i=1,2,\dots,B$ are independent, identically distributed Gaussian random variables with zero mean and a variance of $\frac{N_0}{2}$. The projection of the received signal can be expressed as

$$r(t) = \sum_{i=1}^B B_{ni} \Phi_i(t) \quad (3.14)$$

where $B_{ni} = \sqrt{E} A_{ni} + n_i$

3.5.2 The Modified Viterbi Algorithm and System Simulation

For the Viterbi receiver described in section 2.4.1, we have the metric

$$Z_n(\tilde{\gamma}) = \int_{nT}^{(n+1)T} r(t) S(t, \tilde{\gamma}) dt \quad (3.15)$$

As we insert $r(t)$ of (3.14) and $S(t, \tilde{\gamma})$ of (3.12) into (3.15), and use the fact that $\Phi_1, \Phi_2, \dots, \Phi_B$ are the vectors of an orthonormal basis

$$Z_n(\tilde{\alpha}) = \sqrt{E} \sum_{i=1}^B A_{ni} B_{ni} \quad (3.16)$$

For convolutionally encoded CPFSK system a modified Viterbi algorithm must be used. So, a modified Viterbi

algorithm for the $h=1/4$, $R=1/2$, $(7,2)$ convolutionally encoded CPM system, is used. The state description of a convolutionally encoded CPM system was given in section 2.2.2 and the state vector was given in (2.14). Now, considering the rate $R=1/2$, $(7,2)$ convolutional encoder we have the state vector

$$(\theta_n, \alpha_{n-1}, \alpha_{n-2}) \quad (3.17)$$

where θ_n is the phase at the beginning of the symbol interval and it is given by

$$\theta_n = \left[\pi h \sum_{i=-\infty}^{n-1} \gamma_i \right] \text{ mod } 2\pi \quad (3.18)$$

For our case; α_{n-1} , α_{n-2} are the generated bits at $(n-1)$ 'th and $(n-2)$ 'th symbol intervals respectively as we are at the present, n 'th symbol interval. Note that α_{n-1} and α_{n-2} are the register values of the convolutional encoder at the n 'th symbol interval. As we have $h=1/4$, θ_n can take 8 different values; and since $\alpha_{n-1}, \alpha_{n-2}$ can take the values of 0 or 1, we totally have 32 states. Note in general that the number of states, for a rate $R=\mu/\eta$ convolutionally encoded CPM with $h=2k/p$ and with constraint length v , is given by $S=p2^{\nu\mu(L-1)}$ where L is the modulation pulse length (Ho and McLane, 1988).

The Viterbi algorithm, for the $h=1/4$, $R=1/2$ $(7,2)$ convolutional encoder, works in the same way in principle as the Viterbi algorithm described in section 3.4.1 for uncoded case. The main difference is that, the states of

the receiver consist of two past generated symbols $\alpha_{n-1}, \alpha_{n-2}$. Also the metrics are computed by considering α_n, α_{n-1} and α_{n-2} . The algorithm calculates 32 metrics, for each symbol interval after the initial transition, and half of them is discarded since two paths enter into each state.

We assume that all metrics are initially zero and the algorithm begins with the (0,0,0) state where the initial phase is assumed to be zero. The convolutional encoder registers are also assumed to contain zero initially. We have taken the path memory length N_T to be 50 channel symbol intervals which is again large enough to ensure that all unmerged pairs have a distance greater than MNSED (Lindell et al, 1988). Note that this state structure is in the form of a Markov process which is essential for the application of the Viterbi algorithm (Ho and Mclane, 1988).

In our system, we generate random binary bits {0,1}, we convolutionally encode them with $R=1/2$ (7,2) convolutional encoder and then obtain γ_i according to Table 3.5., we modulate the obtained 4-ary bit γ_i and obtain signal space vectors for the corresponding bit. Then we add an independent, identically distributed Gaussian variate of variance $\frac{N_0}{2}$ onto each component to obtain the received signal. Then the algorithm looks for

the best metric path leading into each state for each symbol interval. There are two paths entering and coming out of each state; and the path giving the smallest metric at each state is deleted. After 50 bit intervals, the receiver begins to decide on the transmitted bits α_i . And then we get the error performance of the receiver by comparing the output symbols with the known transmitted bits α_i .

3.6 Simulation Results

The simulations have performed for $h=1/2$, $h=1/4$ uncoded CPFSK system and $h=1/4$, $R=1/2$, $(7,2)$ convolutionally encoded CPFSK system.

For uncoded binary case the constant C given in (2.26) is equal to 1 (Lindell et al, 1988). The probability of error curve obtained by the simulation, for $h=1/2$ uncoded CPFSK is given with the $Q\left[\sqrt{d_{\min}^2 E_b / N_0}\right]$ curve in Figure 3.6. As it can be seen from the figure, the curves are close to each other. Note that $Q(x)$ can be approximated by

$$Q(x) \leq \frac{1}{2} e^{-x^2/2}$$

for large x (Anderson et al, 1986:21). Note also that $d_{\min}^2 = 2$ for $h=1/2$ case (Anderson et al, 1986:63).

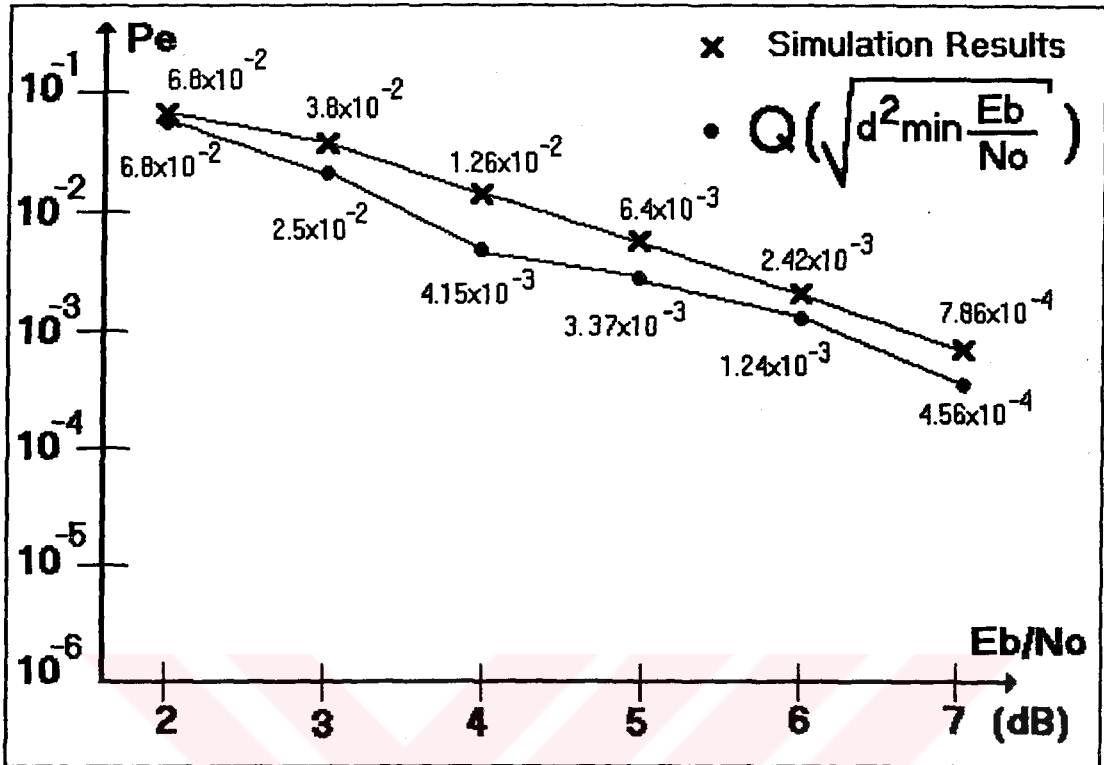


Figure 3.6. Probability of Error Curve for $h=1/2$. Uncoded CPFSK with $Q\left[\sqrt{d_{\min}^2 \frac{E_b}{N_o}}\right]$ Curve.

For $h=1/4$ uncoded CPFSK the probability of error curve obtained by the simulation with the $Q\left[\sqrt{d_{\min}^2 \frac{E_b}{N_o}}\right]$ curve is given in Figure 3.7. As seen from the curve, the results are close to the approximated probability of error curve $Q\left[\sqrt{d_{\min}^2 \frac{E_b}{N_o}}\right]$. Note that $d_{\min}^2=0.72$ for $h=1/4$ case (Anderson et al:63).

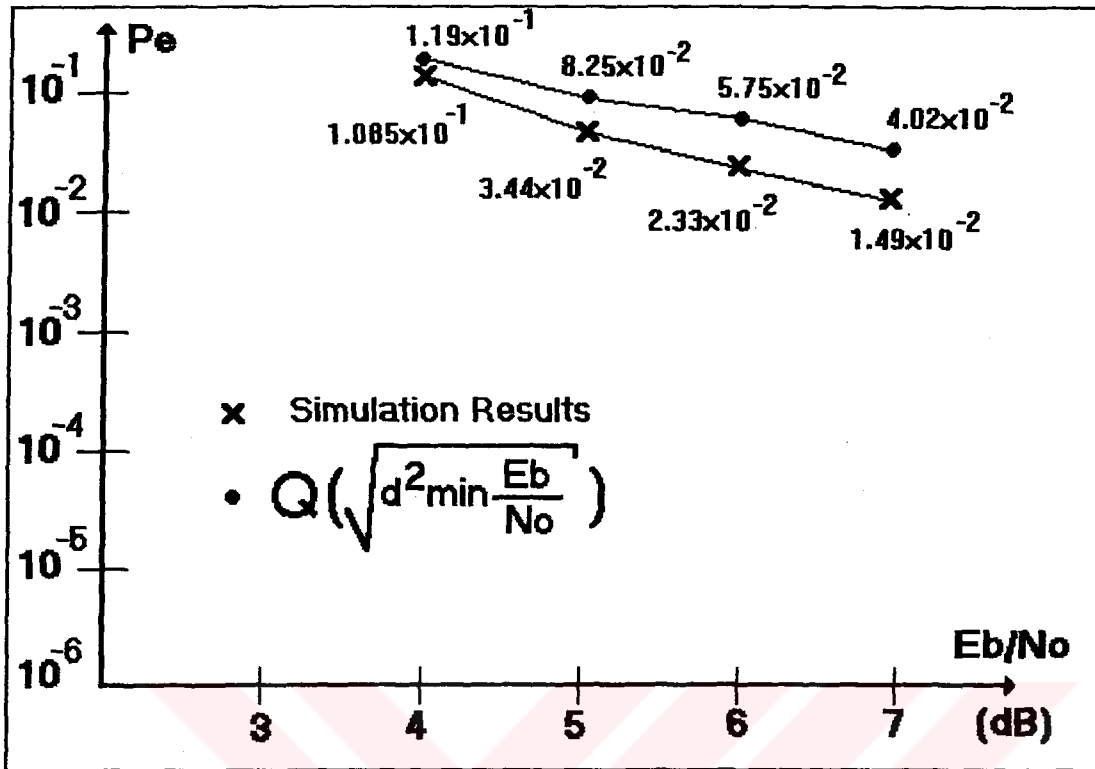


Figure 3.7. Probability of Error Curve for $h=1/4$ Uncoded CPFSK with $Q\left[\sqrt{d_{\min}^2 \frac{E_b}{N_0}}\right]$ Curve.

As it is seen from the simulation curves, given in Figures 3.6 and 3.7, $h=1/2$ uncoded CPFSK has better error performance than $h=1/4$ case. This is expected because, MNSED d_{\min}^2 for $h=1/2$ case is much larger than MNSED for $h=1/4$ case.

For $h=1/4$, rate $R=1/2$, (7,2) convolutionally encoded CPFSK; with $Q\left[\sqrt{d_{\min}^2 \frac{E_b}{N_0}}\right]$ curve, the simulation results obtained are given in Figure 3.8. Note that the constant

C in (2.26) is not exactly equal to 1 for this case but it is approximated to be 1 so that

$$P_e \approx Q \left[\sqrt{d_{\min}^2 E_b / N_0} \right]$$

(Anderson et al, 1986). The curves are close to each other. Note that MNSED is equal to 4.30 as can be seen from Table 3.1.

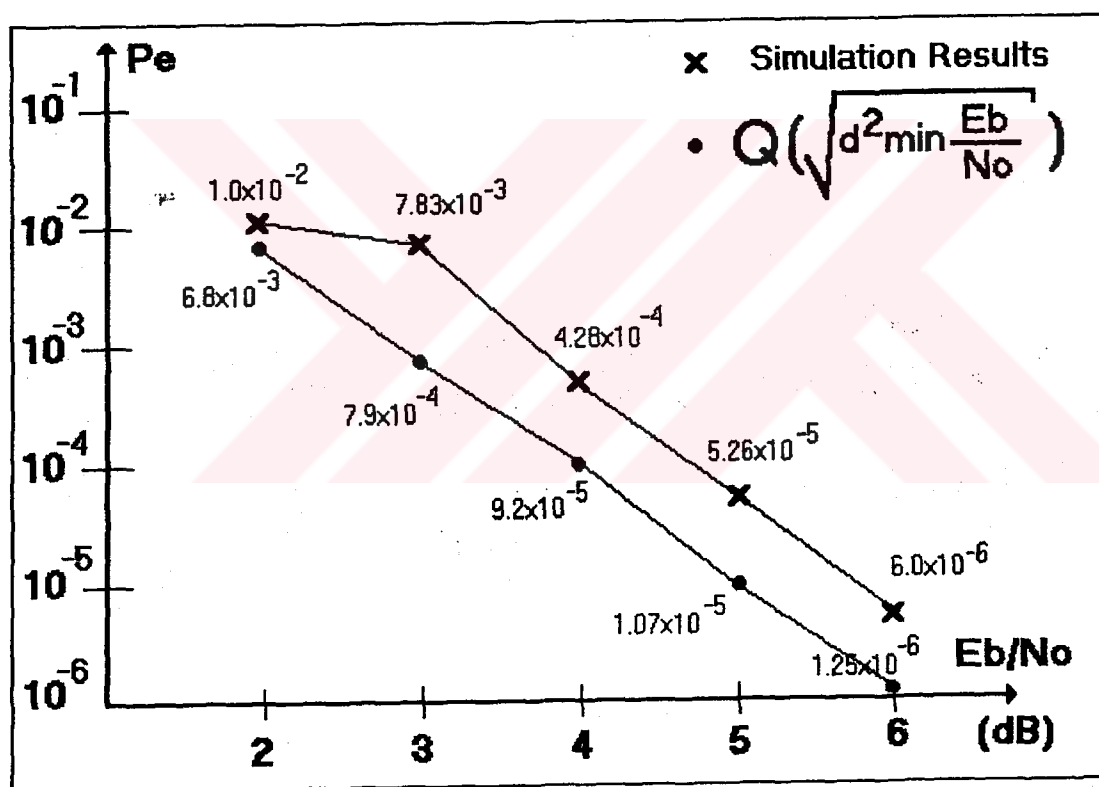


Figure 3.8. Probability of Error Curve for $h=1/4$, $R=1/2$ (7,2) Convolutionally Encoded CPFSK with $Q \left[\sqrt{d_{\min}^2 E_b / N_0} \right]$ Curve.

For comparing the $h=1/4$ uncoded CPFSK and $h=1/4$, $R=1/2$, (7,2) convolutionally encoded CPFSK systems, we give the simulation results together for these cases, in Figure 3.9. As it is seen from the curves, the convolutionally encoded $h=1/4$ CPFSK system has much better error performance than the uncoded $h=1/4$ case. To reach probability of error in the order of 10^{-2} , we need about 7 dB SNR for the uncoded case but for the encoded case we need less than 3 dB SNR for the same probability of bit error.

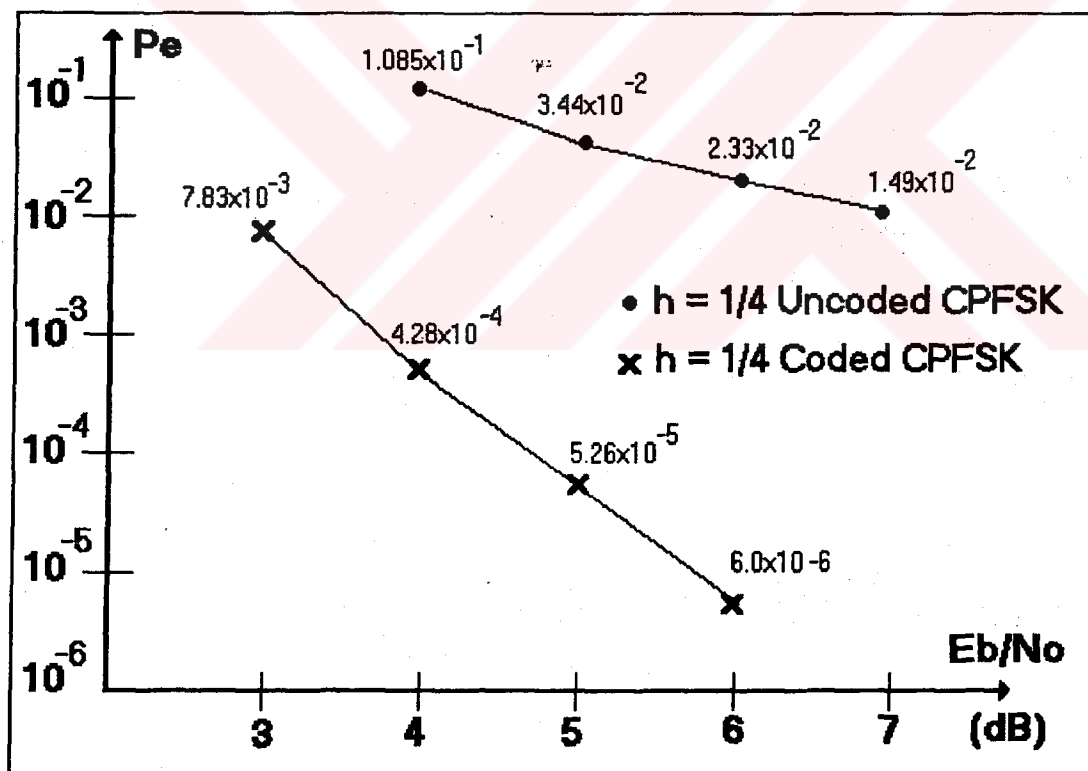


Figure 3.9. Probability of Error Curve for the Uncoded and Encoded CPFSK for $h=1/4$.

So, by convolutionally encoding the CPFSK system for $h=1/4$ case, we increase MNSD so that we get better error performance than the uncoded $h=1/4$ case.



CHAPTER IV

CONCLUSION

In this work, uncoded and convolutionally encoded CPFSK schemes, in the presence of additive white Gaussian noise are studied. Noise is introduced to the modulated signals by the so called signal space method and orthonormal bases are derived both for the uncoded and the encoded CPFSK schemes. The four dimensional basis for binary uncoded CPFSK, given by the equations (3.5.a) to (3.5.d) can also be obtained as a special case of the basis for binary uncoded multi-h CPFSK schemes given in (Anderson et al, 1986). Table 3.2 which shows the signal vector coefficients is prepared for uncoded modulating signals that can be used for any modulation index h . Also all transmitted vectors for the modulation indices $h=1/2$ and $h=1/4$ are given in Table 3.3 and Table 3.4 respectively.

The eight dimensional basis derived in this work given by equations (3.11.a) to (3.11.h) appears in literature for the first time (see Appendix B for the

details). Also the signal vector coefficients for the eight dimensional case are calculated and tabulated in Table 3.6 for rate $R=1/2$ (7,2) convolutionally encoded CPFSK signals. The table can be used for any rate $R=1/2$ convolutionally encoded CPFSK scheme as well.

The bit error probabilities for the simulated 3 cases are obtained by computer simulations. The computer simulations show that the error performance, for uncoded CPFSK, gets better as h is increased from $h=1/4$ to $h=1/2$. Furthermore as we convolutionally encode the CPFSK signals, we have larger minimum normalized squared Euclidean distance and as seen from the simulation results, we achieve much better bit error probability rates. By convolutionally encoding CPFSK signals, about 4 dB SNR gain can be obtained to achieve the same error probability.

It must be noted that, the orthonormal basis and the modulation signal tables obtained are necessary to use the signal space method, for the introduction of channel noise. The orthonormal basis obtained for the rate $R=1/2$ (7,2) convolutionally encoded CPFSK system, and the table obtained for the modulated signals can be used directly for any, rate $R=1/2$ convolutional encoder. Also this table can be used for any modulation index h . If the rate R is increased, the signal space dimension will also be

increased. For $R=2/3$ case the dimension will be 16, and it must be noted that to obtain 16 dimensional orthonormal basis will be quite complicated.

Finally note that, the obtained tables can be used not only for AWGN channels but for some other channels. For example it can be used for a fading mobile channel where the modulated signal is normalized by a random fading amplitude in a symbol interval. The performance analysis of several, rate $R=1/2$, convolutional codes for AWGN channels and other applicable channels may be proposed for future studies.

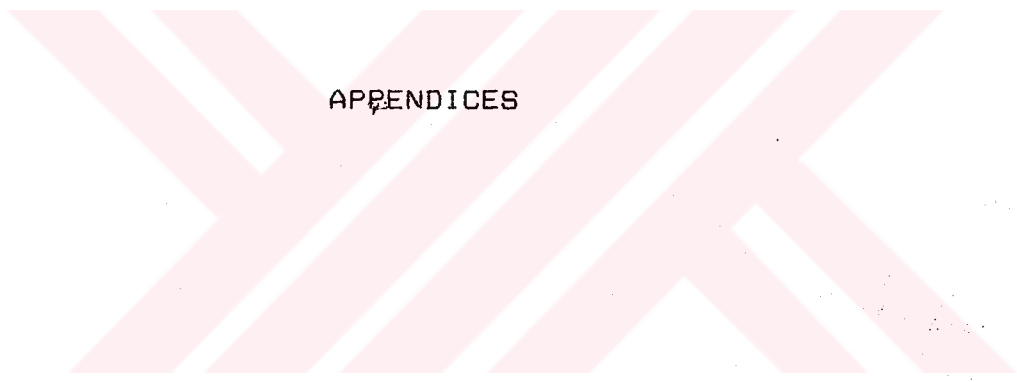
REFERENCES

- Anderson, J.B., 1981. "Simulated Error Performance of Multi-h Phase Codes", IEEE Trans. Inform. Theory, Vol. IT-27, pp. 357-362.
- Anderson, J.B., Aulin, T., Sundberg C., 1986. Digital Phase Modulation. New York: Plenum.
- Aulin, T. and Sundberg, C.W. 1981a. "Continuous Phase Modulation-Part I: Full Response Signalling", IEEE Trans. Commun., Vol. COM-29, pp. 196-209.
- Aulin, T., Rydbeck, N. and Sundberg, C.W. 1981b. "Continuous Phase Modulation-Part II: Partial Response Signalling", IEEE Trans. Commun., Vol. COM-29, pp. 210-225.
- Aulin, T., 1981. "Symbol Error Probability Bounds for Coherently Viterbi Detected Continuous Phase Modulated Signals", IEEE Trans. Commun., Vol. COM-29, pp. 1707-1715.
- Forney, G.D., 1973. "The Viterbi Algorithm", Proceedings of IEEE, Vol. 61, pp. 268-278.
- Haykin, Simon, 1978. Communication Systems, New York: John Wiley & Sons.
- Ho, P.K.M. and McLane, P.J., 1988. "Spectrum, Distance and Receiver Complexity of Encoded Continuous Phase Modulation", IEEE Trans. Inform. Theory, Vol. 34, NO. 5, pp. 1021-1032.

- Kaleh, G.K., 1989. "Simple Coherent Receivers for Partial Response Continuous Phase Modulation", IEEE Jour. Sel. Areas in Commun., Vol.7, pp. 1427-1436.
- Lindell, G. and Sundberg, C.W., 1988. "An upper Bound on the Bit Error Probability of Combined Convolutional Coding and Continuous Phase Modulation", IEEE Trans. Inform. Theory, Vol. 34, NO.5, pp. 1263-1269.
- Lindell, G., Sundberg, C. and Aulin, T., 1984. "Minimum Euclidean Distance for Combinations of Short Rate $1/2$ Convolutional Codes and CPFSK Modulation", IEEE Trans. Inform. Theory, Vol. IT-30, pp. 509-519.
- Mulligan, M.G. and Wilson, S.G., 1984. "An Improved Algorithm for Evaluating Trellis Phase Codes", IEEE Trans. Inform. Theory, Vol. IT-30, pp. 846-851.
- Osborne, W.P. and Lutz, M.B., 1974. "Coherent and Noncoherent Detection of CPFSK", IEEE Trans. Commun., Vol. COM-22, pp. 1023-1036.
- Paula, R.F. and Golden, R., 1981. "Simulations of Convolutional Coding/Viterbi Decoding with Noncoherent CPFSK", IEEE Trans. Commun., Vol. COM-29, pp. 1522-1526.
- Pizzi, S.V. and Wilson S.G., 1985. "Convolutional Coding Combined with Continuous Phase Modulation", IEEE Trans. Commun., Vol. COM-33, pp. 20-29.
- Press, W.H., Flannery, B.P., Teukolsky, S.A., Vetterling, W.T., 1988. Numerical Recipes in C., New York, Cambridge University Press.

Proakis J., 1989. Digital Communications, Singapore
McGraw-Hill.



A decorative horizontal band featuring a series of parallel diagonal stripes in a light pink or rose color, alternating with white space. The stripes are slanted at approximately 45 degrees.

APPENDICES

APPENDIX A

DISTANCE CALCULATIONS FOR THE TWO PATH GIVEN IN FIGURE 3.2. FOR SEVERAL MODULATION INDICES

A.1 Calculation of $d_{12}^2(4)$ for the Two Path Given in Figure 3.2 for $h=3/10$

For $h=3/10$, $R=1/2$, (7,2) convolutionally encoded
CPFSK

$$\begin{aligned}d_{12}^2(4) &= \frac{1}{2E} \int_0^{4T} [S_1(t) - S_2(t)]^2 dt \\ &= \frac{1}{T} \int_0^{4T} [1 - \cos \Delta \Phi(t)] dt\end{aligned}$$

For the first interval:

$$\begin{aligned}d_{12}^2(1) &= \frac{1}{T} \int_0^T \left[1 - \cos \left(\frac{t}{T} \pi h (\gamma_0 - \gamma'_0) \right) \right] dt \\ &= \frac{1}{T} \int_0^T \left[1 - \cos \left(\frac{12\pi t}{T} \right) \right] dt \\ &= 1.15591\end{aligned}$$

For the second interval:

$$\begin{aligned}
d_{12}^2(2) &= d_{12}^2(1) + \frac{1}{T} \int_0^T \left[1 - \cos \left(\frac{12\pi}{10} + \frac{3\pi}{10} \frac{(t-T)}{T} \right) \right] dt \\
&= d_{12}^2(1) + \frac{10}{6\pi} \left[1 - \left[\sin \frac{18\pi}{10} - \sin \frac{12\pi}{10} \right] \right] \\
&= d_{12}^2(1) + 1 \\
&= 2.15591
\end{aligned}$$

For the third interval:

$$\begin{aligned}
d_{12}^2(3) &= d_{12}^2(2) + \frac{1}{T} \int_{2T}^{3T} \left[1 - \cos \left(\frac{3\pi}{10} - \frac{3\pi}{10} 2 \frac{(t-2T)}{T} \right) \right] dt \\
&= d_{12}^2(2) + \left[1 + \frac{10}{6\pi} \left[\sin \frac{12\pi}{10} - \sin \frac{18\pi}{10} \right] \right] \\
&= 1 + d_{12}^2(2) \\
&= 3.15591
\end{aligned}$$

For the fourth interval:

$$\begin{aligned}
d_{12}^2(4) &= d_{12}^2(3) + \frac{1}{T} \int_{3T}^{4T} \left[1 - \cos \left(\frac{12\pi}{10} - \frac{3\pi}{10} 4 \frac{(t-3T)}{T} \right) \right] dt \\
&= d_{12}^2(3) + \left[1 - \frac{10}{12\pi} \sin \frac{12\pi}{10} \right] \\
&= d_{12}^2(3) + 1.15591 \\
&= 4.31182
\end{aligned}$$

A.2 Calculation of $d_{12}^2(4)$ for the Two Path Given in Figure 3.2 for $h=1/4$

For $h=1/4$, $R=1/2$, (7,2) convolutionally encoded CPFSK:

For the first interval:

$$d_{12}^2(1) = \frac{1}{T} \int_0^T \left[1 - \cos \left(\frac{t}{T} - \frac{\pi}{4} 4 \right) \right] dt$$

$$= \frac{1}{T} \left[T - \frac{T}{\pi} \sin\left(\frac{\pi t}{T}\right) \right]$$

$$= 1$$

For the second interval:

$$d_{12}^2(2) = d_{12}^2(1) + \frac{1}{T} \left[T - \sin\left(\frac{\pi t}{2T}(t-T) + \pi\right) \right] \frac{2T}{\pi}$$

$$= d_{12}^2(1) + \left[1 - \sin\left(\frac{\pi}{2} + \pi\right) \right] \frac{2}{\pi}$$

$$= 2.636$$

For the third interval:

$$d_{12}^2(3) = d_{12}^2(2) + \frac{1}{T} \int_{2T}^{3T} \left[1 - \cos\left(\frac{\pi}{4} t - \frac{\pi}{4} 2 \frac{(t-2T)}{T}\right) \right] dt$$

$$= d_{12}^2(2) - \frac{2}{\pi} \left[1 - \left[\sin \frac{4\pi}{4} - \sin \frac{6\pi}{4} \right] \right]$$

$$= 4.2732$$

For the fourth interval:

$$d_{12}^2(4) = d_{12}^2(3) + \frac{1}{T} \int_{3T}^{4T} \left[1 - \cos\left(\frac{4\pi}{4} t - \frac{\pi}{4} 4 \frac{(t-3T)}{T}\right) \right] dt$$

$$= d_{12}^2(3) + 1$$

$$= 5.273$$

A.3 Calculation of $d_{12}^2(4)$ for the Two Path Given in Figure 3.2 for $h=1/6$

For $h=1/6$, $R=1/2$, $(7,2)$ convolutionally encoded CPFSK, for the first interval:

$$d_{12}^2(1) = \frac{1}{T} \left[T - \sin\left(\frac{\pi}{6} t\right) \right] \frac{6T}{4\pi}$$

$$= 0.586$$

For the second interval:

$$\begin{aligned}d_{12}^2(2) &= d_{12}^2(1) + \left[1 - \left(\sin\left(\frac{4\pi}{6} + \frac{2\pi}{6}\right) - \sin\left(\frac{4\pi}{6}\right) \right) \frac{6}{2\pi} \right] \\ &= 2\end{aligned}$$

For the third interval:

$$\begin{aligned}d_{12}^2(3) &= d_{12}^2(2) + \left[1 - \left(\sin\left(\pi - \frac{2\pi}{6}\right) - \sin(\pi) \right) \frac{6}{2\pi} \right] \\ &= 3.826\end{aligned}$$

For the fourth interval:

$$\begin{aligned}d_{12}^2(4) &= d_{12}^2(3) + \left[1 - \left(\sin\left(\frac{4\pi}{6} - \frac{4\pi}{6}\right) + \sin\left(\frac{4\pi}{6}\right) \right) \frac{6}{2\pi} \right] \\ &= -\frac{6}{4\pi} \sin\left(\frac{4\pi}{6}\right) + d_{12}^2(3) \\ &= 3.4125\end{aligned}$$

APPENDIX B

DERIVATION OF THE 8 AND 4 DIMENSIONAL ORTHONORMAL BASIS FOR MODULATING SIGNALS

We have the eight modulating signals:

$$S_1(t) = \sqrt{\frac{2}{T}} \cos\left(\omega_c t + \frac{\pi h t}{T}\right)$$

$$S_2(t) = \sqrt{\frac{2}{T}} \sin\left(\omega_c t + \frac{\pi h t}{T}\right)$$

$$S_3(t) = \sqrt{\frac{2}{T}} \cos\left(\omega_c t - \frac{\pi h t}{T}\right)$$

$$S_4(t) = \sqrt{\frac{2}{T}} \sin\left(\omega_c t - \frac{\pi h t}{T}\right)$$

$$S_5(t) = \sqrt{\frac{2}{T}} \cos\left(\omega_c t + \frac{3\pi h t}{T}\right)$$

$$S_6(t) = \sqrt{\frac{2}{T}} \sin\left(\omega_c t + \frac{3\pi h t}{T}\right)$$

$$S_7(t) = \sqrt{\frac{2}{T}} \cos\left(\omega_c t - \frac{3\pi h t}{T}\right)$$

$$S_8(t) = \sqrt{\frac{2}{T}} \sin\left(\omega_c t - \frac{3\pi h t}{T}\right)$$

where $0 \leq t \leq T$.

The Gram-Schmidt procedure is used to form an orthonormal basis for these signals (Haykin, 1978). For the first pair of orthonormal basis, we choose the pair of signals

$$\Phi_1(t) = \sqrt{\frac{2}{T}} \cos\left(\omega_c t + \frac{\pi h t}{T}\right) \quad (\text{B.1})$$

$$\Phi_2(t) = \sqrt{\frac{2}{T}} \sin\left(\omega_c t + \frac{\pi h t}{T}\right) \quad (\text{B.2})$$

These signals are of unit energy, and as $\omega_c \rightarrow \infty$, $(\Phi_1, \Phi_2) \rightarrow 0$. Here $(u, v) = \int_0^T u(t) v(t) dt$.

For the second pair, we begin with the pair

$$S_3(t) = \sqrt{\frac{2}{T}} \cos\left(\omega_c t - \frac{\pi h t}{T}\right) \quad (\text{B.3})$$

$$S_4(t) = \sqrt{\frac{2}{T}} \sin\left(\omega_c t - \frac{\pi h t}{T}\right) \quad (\text{B.4})$$

These are mutually orthogonal in the sense that $(S_3, S_4) \rightarrow 0$ as $\omega_c \rightarrow \infty$, but not orthogonal to Φ_1 and Φ_2 . From the Gram-Schmidt procedure (Haykin, 1978), come $\theta_3(t)$ and $\theta_4(t)$ which are orthogonal,

$$\theta_3(t) = S_3(t) - b_{31}\Phi_1(t) - b_{32}\Phi_2(t) \quad (\text{B.5})$$

$$\theta_4(t) = S_4(t) - b_{41}\Phi_1(t) - b_{42}\Phi_2(t) - b_{43}\Phi_3(t) \quad (\text{B.6})$$

where $b_{31} = (S_3, \Phi_1)$, $b_{32} = (S_3, \Phi_2)$ and $b_{41} = (S_4, \Phi_1)$, $b_{42} = (S_4, \Phi_2)$ and $b_{43} = (S_4, \Phi_3)$.

$$b_{31} = \int_0^T \left[\frac{2}{T}\right] \cos\left[\omega_c t - \frac{\pi h t}{T}\right] \cos\left[\omega_c t + \frac{\pi h t}{T}\right] dt$$

$$\begin{aligned}
&= \frac{1}{T} \int_0^T \left[\cos(2\omega_c t) + \cos\left(\frac{2\pi h t}{T}\right) \right] dt \\
&= \frac{1}{T} \left[\frac{1}{2\omega_c} \sin(2\omega_c T) + \frac{T}{2\pi h} \sin(2\pi h) \right]
\end{aligned}$$

and as $\omega_c \gg \frac{1}{T}$ we have

$$b_{31} = \frac{\sin(2\pi h)}{2\pi h} = S_o \quad (\text{B.7})$$

$$\begin{aligned}
b_{32} &= \int_0^T \left(\frac{2}{T}\right) \cos\left[\omega_c t - \frac{\pi h t}{T}\right] \sin\left[\omega_c t - \frac{\pi h t}{T}\right] dt \\
&= \frac{2}{T} \int_0^T \frac{1}{2} \left[\sin(2\omega_c t) + \sin\left(\frac{2\pi h t}{T}\right) \right] dt \\
&= \frac{1}{T} \left[\frac{1}{2\omega_c} (1 - \cos(2\omega_c T)) + \frac{T}{2\pi h} (1 - \cos(2\pi h)) \right]
\end{aligned}$$

as $\omega_c \gg \frac{1}{T}$ we have

$$b_{32} = \frac{1 - \cos(2\pi h)}{2\pi h} = C_o \quad (\text{B.8})$$

$$\begin{aligned}
b_{41} &= \int_0^T \left(\frac{2}{T}\right) \sin\left[\omega_c t - \frac{\pi h t}{T}\right] \cos\left[\omega_c t + \frac{\pi h t}{T}\right] dt \\
&= \frac{2}{T} \int_0^T \frac{1}{2} \left[\sin(2\omega_c t) - \sin\left(\frac{2\pi h t}{T}\right) \right] dt \\
&= \frac{1}{T} \left[\frac{1}{2\omega_c} (1 - \cos(2\omega_c T)) + \frac{T}{2\pi h} (\cos(2\pi h) - 1) \right]
\end{aligned}$$

as $\omega_c \gg \frac{1}{T}$ we have

$$b_{41} = \frac{\cos(2\pi h) - 1}{2\pi h} = -C_o \quad (\text{B.9})$$

$$b_{42} = \int_0^T \left[\frac{2}{T} \right] \sin \left[\omega c t - \frac{\pi h t}{T} \right] \sin \left[\omega c t + \frac{\pi h t}{T} \right] dt$$

$$= \frac{2}{T} \int_0^T \frac{1}{2} \left[\cos \left(\frac{2\pi h t}{T} \right) - \cos(2\omega c t) \right] dt$$

as $\omega c \gg \frac{1}{T}$ we have

$$b_{42} = \frac{\sin(2\pi h)}{2\pi h} = S_0 \quad (\text{B.10})$$

Now, define

$$\Phi_3(t) = \frac{\theta_3(t)}{|\theta_3|} \quad (\text{B.11.a})$$

$$\Phi_4(t) = \frac{\theta_4(t)}{|\theta_4|} \quad (\text{B.11.b})$$

where $|\theta_3|$ and $|\theta_4|$ are constants making the energy of $\Phi_3(t)$ and $\Phi_4(t)$ unity respectively, so that

$$\int_0^T \Phi_3^2(t) dt = \int_0^T \Phi_4^2(t) dt = 1$$

In other words, $\Phi_3(t)$ and $\Phi_4(t)$ are the normalized forms of $\theta_3(t)$ and $\theta_4(t)$ respectively.

Using the fact that $S_3(t)$ and $S_4(t)$ are orthogonal

$$b_{43} = \frac{1}{|\theta_3|} \int_0^T \left[\sqrt{\frac{2}{T}} \sin \left[\omega c t - \frac{\pi h t}{T} \right] \right]$$

$$\left[\sqrt{\frac{2}{T}} \cos \left[\omega c t - \frac{\pi h t}{T} \right] - S_0 \Phi_1(t) - C_0 \Phi_2(t) \right] dt$$

$$\begin{aligned}
&= \frac{1}{|\theta_3|} \int_0^T \left[\sqrt{\frac{2}{T}} \sin\left(\omega_c t - \frac{\pi h t}{T}\right) \right] \left[-s_o \Phi_1(t) - c_o \Phi_2(t) \right] dt \\
&= (-b_{41} s_o - b_{42} c_o) \frac{1}{|\theta_3|} = 0 \quad (B.12)
\end{aligned}$$

To find $\Phi_3(t)$ and $\Phi_4(t)$ we must obtain $|\theta_3|$ and $|\theta_4|$:

$$\begin{aligned}
|\theta_3|^2 &= \int_0^T \theta_3^2(t) dt \\
&= \int_0^T \left[s_3(t) - b_{31} \Phi_1(t) - b_{32} \Phi_2(t) \right]^2 dt \\
&= \int_0^T \left[s_3^2(t) - b_{31}^2 - b_{32}^2 \right] dt = (1 - b_{31}^2 - b_{32}^2)
\end{aligned}$$

so we have

$$|\theta_3| = (1 - s_o - c_o)^{1/2} = D_1 \quad (B.13)$$

similarly

$$|\theta_4|^2 = \int_0^T \theta_4^2(t) dt = 1 - b_{41}^2 - b_{42}^2$$

than

$$|\theta_4| = (1 - c_o - s_o)^{1/2} = D_1 \quad (B.14)$$

And using equations (B.7) to (B.14) we have :

$$\begin{aligned}
\Phi_3(t) &= \frac{s_3(t) - b_{31} \Phi_1(t) - b_{32} \Phi_2(t)}{D_1} \\
&= \frac{s_3(t) - s_o \Phi_1(t) - c_o \Phi_2(t)}{D_1} \quad (B.15)
\end{aligned}$$

$$\Phi_4(t) = \frac{s_4(t) - b_{41} \Phi_1(t) - b_{42} \Phi_2(t)}{D_1}$$

$$\Phi_4(t) = \frac{S_4(t) + C_o \Phi_1(t) - S_o \Phi_2(t)}{D_1} \quad (\text{B.16})$$

Now, we have obtained four orthonormal functions, $\Phi_1(t)$, $\Phi_2(t)$, $\Phi_3(t)$ and $\Phi_4(t)$, corresponding to the four modulating signals $S_1(t)$, $S_2(t)$, $S_3(t)$ and $S_4(t)$ respectively. Note that, these four orthonormal functions create the four dimensional orthonormal basis for uncoded 2 level CPFSK.

We continue to create orthonormal functions for the third pair, and we begin with

$$S_5(t) = \sqrt{\frac{2}{T}} \cos\left(\omega_c t + \frac{3\pi h t}{T}\right)$$

$$S_6(t) = \sqrt{\frac{2}{T}} \sin\left(\omega_c t + \frac{3\pi h t}{T}\right)$$

To make this pair orthogonal to, $\Phi_1(t)$, $\Phi_2(t)$, $\Phi_3(t)$ and $\Phi_4(t)$; we have $\theta_5(t)$ and $\theta_6(t)$ which are orthogonal from the Gram-Schmidt procedure :

$$\theta_5(t) = S_5(t) - b_{51}\Phi_1(t) - b_{52}\Phi_2(t) - b_{53}\Phi_3(t) - b_{54}\Phi_4(t)$$

$$\theta_6(t) = S_6(t) - b_{61}\Phi_1(t) - b_{62}\Phi_2(t) - b_{63}\Phi_3(t) - b_{64}\Phi_4(t) - b_{65}\Phi_5(t)$$

$\theta_5(t)$ and $\theta_6(t)$ are mutually orthogonal but not of unit energy, to normalize them we have

$$\Phi_5(t) = \frac{\theta_5(t)}{|\theta_5|} \quad (\text{B.17})$$

$$\Phi_6(t) = \frac{\theta_6(t)}{|\theta_6|} \quad (\text{B.18})$$

where

$$|\theta_5| = (1 - b_{51}^2 - b_{52}^2 - b_{53}^2 - b_{54}^2)^{1/2} \quad (\text{B.19})$$

$$|\theta_6| = (1 - b_{61}^2 - b_{62}^2 - b_{63}^2 - b_{64}^2 - b_{65}^2)^{1/2} \quad (\text{B.20})$$

From now on, as it is assumed that $Wc \gg \frac{1}{T}$ the terms multiplying $\frac{Wc}{T}$ are deleted.

$$\begin{aligned} b_{51} &= \int_0^T \left(\frac{2}{T} \right) \cos \left(Wct + \frac{3\pi ht}{T} \right) \cos \left(Wct + \frac{\pi ht}{T} \right) dt \\ &= \int_0^T \left(\frac{1}{T} \right) \left[\cos \left(2Wct + \frac{4\pi ht}{T} \right) + \cos \left(\frac{2\pi ht}{T} \right) \right] dt \\ &= \frac{\sin(2\pi h)}{2\pi h} = S_o \end{aligned}$$

so,

$$b_{51} = S_o \quad (\text{B.21})$$

$$\begin{aligned} b_{51} &= \int_0^T \left(\frac{2}{T} \right) \cos \left(Wct + \frac{3\pi ht}{T} \right) \sin \left(Wct + \frac{\pi ht}{T} \right) dt \\ &= \frac{2}{T} \int_0^T \left(\frac{1}{2} \right) \left[\sin \left(2Wct + \frac{4\pi ht}{T} \right) - \sin \left(\frac{2\pi ht}{T} \right) \right] dt \\ &= \frac{\cos(2\pi h) - 1}{2\pi h} \end{aligned}$$

$$b_{52} = -C_o \quad (\text{B.22})$$

$$\begin{aligned} b_{53} &= \int_0^T S_5(t) \Phi_3(t) dt \\ &= \int_0^T S_5(t) \left[\frac{S_3(t) - b_{31}\Phi_1(t) - b_{32}\Phi_2(t)}{D_1} \right] dt \end{aligned}$$

$$\begin{aligned}
&= \frac{1}{D_1} \left[\int_0^T \left(\frac{2}{T} \right) \cos \left(\omega t - \frac{\pi h t}{T} \right) \cos \left(\omega t + \frac{3\pi h t}{T} \right) dt \right. \\
&\quad \left. - b_{31} b_{51} - b_{32} b_{52} \right] \\
&= \frac{1}{D_1} \left[\int_0^T \left(\frac{1}{T} \right) \cos \left(\frac{4\pi h t}{T} \right) dt - S_0^2 + C_0^2 \right]
\end{aligned}$$

so
$$b_{53} = \frac{1}{D_1} [S_1 - S_0^2 - C_0^2] \quad (B.23)$$

where
$$S_1 = \frac{\sin(4\pi h)}{4\pi h} \quad (B.24)$$

$$\begin{aligned}
b_{54} &= \int_0^T S_5(t) \Phi_4(t) dt \\
&= \int_0^T S_5(t) \left[\frac{S_4(t) - b_{41} \Phi_1(t) - b_{42} \Phi_2(t)}{D_1} \right] dt \\
&= \frac{1}{D_1} \left[\int_0^T S_5(t) S_4(t) dt - b_{41} b_{51} - b_{42} b_{52} \right] \quad (B.25)
\end{aligned}$$

and we have

$$\begin{aligned}
\int_0^T S_5(t) S_4(t) dt &= \int_0^T \left(\frac{2}{T} \right) \cos \left(\omega t + \frac{3\pi h t}{T} \right) \sin \left(\omega t - \frac{\pi h t}{T} \right) dt \\
&= \int_0^T \left(\frac{1}{T} \right) \sin \left(- \frac{4\pi h t}{T} \right) dt = \frac{\cos(4\pi h) - 1}{4\pi h} \\
\text{we have } \int_0^T S_5(t) S_4(t) dt &= -C_1 \quad (B.27)
\end{aligned}$$

Now as we put equations, (B.27), (B.9), (B.10), (B.21) and (B.22) into equation (B.25) we have

$$b_{54} = \frac{2C_o S_o - C_1}{D_1} \quad (B.28)$$

Now putting b_{51} , b_{52} into equation (B.19) we obtain

$$|\theta_5| = (1 - S_o^2 - C_o^2 - b_{53}^2 - b_{54}^2)^{1/2} \text{ and define}$$

$$D_2 = (1 - S_o^2 - C_o^2 - b_{53}^2 - b_{54}^2)^{1/2} \quad (B.29)$$

so that $|\theta_5| = D_2$, using (B.17), b_{51} , b_{52} we have

$$\Phi_5(t) = \frac{S_5(t) - S_o \Phi_1(t) + C_o \Phi_2(t) - b_{53} \Phi_3(t) - b_{54} \Phi_4(t)}{D_2} \quad (B.30)$$

For the sixth vector we have:

$$\begin{aligned} b_{61} &= \int_0^T S_6(t) \Phi_1(t) dt \\ &= \int_0^T \left[\frac{2}{T} \right] \sin\left[\omega ct + \frac{3\pi ht}{T}\right] \cos\left[\omega ct + \frac{\pi ht}{T}\right] dt \\ &= \int_0^T \left[\frac{1}{T} \right] \sin\left[\frac{2\pi ht}{T}\right] dt = \frac{1 - \cos(2\pi h)}{2\pi h} = C_o \end{aligned}$$

so $b_{61} = C_o \quad (B.31)$

$$\begin{aligned} b_{62} &= \int_0^T S_6(t) \Phi_2(t) dt \\ &= \int_0^T \left[\frac{2}{T} \right] \sin\left[\omega ct + \frac{3\pi ht}{T}\right] \sin\left[\omega ct + \frac{\pi ht}{T}\right] dt \\ &= \int_0^T \left[\frac{1}{T} \right] \cos\left[\frac{2\pi ht}{T}\right] dt = \frac{\sin(2\pi h)}{2\pi h} = S_o \end{aligned}$$

so we have $b_{62} = S_o \quad (B.32)$

$$\begin{aligned}
b_{63} &= \int_0^T S_6(t) \Phi_3(t) dt \\
&= \int_0^T S_6(t) \left[\frac{S_3(t) - b_{31}\Phi_1(t) - b_{32}\Phi_2(t)}{D_1} \right] dt \\
&= \frac{1}{D_1} \left[\int_0^T S_6(t) S_3(t) dt - b_{31}b_{61} - b_{32}b_{62} \right]
\end{aligned}$$

Here,

$$\begin{aligned}
\int_0^T S_6(t) S_3(t) dt &= \int_0^T \left(\frac{2}{T} \right) \sin \left(\omega ct + \frac{3\pi ht}{T} \right) \cos \left(\omega ct - \frac{\pi ht}{T} \right) dt \\
&= \int_0^T \left(\frac{1}{T} \right) \sin \left(\frac{4\pi ht}{T} \right) dt = \frac{1 - \cos(4\pi h)}{4\pi h} = C_1 \quad (B.34)
\end{aligned}$$

so inserting b_{31} , b_{32} , b_{61} , b_{62} and (B.25) into equation (B.24) we have

$$b_{63} = \frac{C_1 - 2C_0 S_0}{D_1} = -b_{54} \quad (B.35)$$

$$\begin{aligned}
b_{64} &= \int_0^T S_6(t) \Phi_4(t) dt \\
&= \int_0^T S_6(t) \left[\frac{S_4(t) - b_{41}\Phi_1(t) - b_{42}\Phi_2(t)}{D_1} \right] dt \\
&= \frac{1}{D_1} \left[\int_0^T S_6(t) S_4(t) dt - b_{41}b_{61} - b_{42}b_{62} \right] \quad (B.36)
\end{aligned}$$

Here

$$\begin{aligned}
\int_0^T S_6(t) S_4(t) dt &= \int_0^T \left[\frac{2}{T} \right] \sin \left[\omega t + \frac{3\pi h t}{T} \right] \sin \left[\omega t - \frac{\pi h t}{T} \right] dt \\
&= \int_0^T \left[\frac{1}{T} \right] \cos \left[\frac{4\pi h t}{T} \right] dt \\
&= \frac{\sin(4\pi h)}{4\pi h} = S_1
\end{aligned} \tag{B.37}$$

Now as we put b_{61} , b_{62} , b_{41} , b_{42} and equation (B.37) into equation (B.36) we have

$$b_{64} = \frac{S_1 + C_0^2 - S_0^2}{D_1} = b_{53} \tag{B.38}$$

$$b_{65} = \int_0^T S_6(t) \Phi_5(t) dt$$

by using equation (B.21) and remembering that $S_5(t)$ and $S_6(t)$ are orthogonal to each other we have

$$\begin{aligned}
b_{65} &= \frac{1}{D_2} \int_0^T S_6(t) \left[S_5(t) - S_0 \Phi_1(t) + C_0 \Phi_2(t) - b_{53} \Phi_3(t) \right. \\
&\quad \left. - b_{54} \Phi_4(t) \right] dt \\
&= \frac{1}{D_2} \left[-S_0 b_{61} + C_0 b_{62} - b_{53} b_{63} - b_{54} b_{64} \right] \\
&= \frac{1}{D_2} \left[-S_0 C_0 + C_0 S_0 + b_{53} b_{54} - b_{54} b_{53} \right] = 0
\end{aligned}$$

Now, we can write $\Phi_6(t)$ using the found coefficients b_{61} through b_{65} , in equation (B.18) we have

$$\Phi_6(t) = \frac{\theta_6(t)}{|\theta_6|}$$

where $|\theta_6| = (1 - C_0^2 - S_0^2 - b_{54}^2 - b_{53}^2)^{1/2} = D_2$, that is seen

from equation (B.29). Note that $|\theta_6|$ is obtained from (B.20). So, we have

$$\Phi_6(t) = \frac{S_6(t) - c_0 \Phi_1(t) - s_0 \Phi_2(t) + b_{54} \Phi_3(t) - b_{53} \Phi_4(t)}{D_2} \quad (\text{B.39})$$

We continue to create orthonormal functions for the fourth pair, and we begin with

$$S_7(t) = \sqrt{\frac{2}{T}} \cos\left(\omega_c t - \frac{3\pi h t}{T}\right)$$

$$S_8(t) = \sqrt{\frac{2}{T}} \sin\left(\omega_c t - \frac{3\pi h t}{T}\right)$$

To make this pair orthogonal to $\Phi_1(t), \Phi_2(t), \dots, \Phi_6(t)$; we have $\theta_7(t)$ and $\theta_8(t)$ which are orthogonal from the Gram-Schmidt procedure.

$$\theta_7(t) = \left[S_7(t) - b_{71} \Phi_1(t) - b_{72} \Phi_2(t) - b_{73} \Phi_3(t) - b_{74} \Phi_4(t) - b_{75} \Phi_5(t) - b_{76} \Phi_6(t) \right] \quad (\text{B.40})$$

$$\theta_8(t) = \left[S_8(t) - b_{81} \Phi_1(t) - b_{82} \Phi_2(t) - b_{83} \Phi_3(t) - b_{84} \Phi_4(t) - b_{85} \Phi_5(t) - b_{86} \Phi_6(t) - b_{87} \Phi_7(t) \right] \quad (\text{B.41})$$

$\theta_7(t)$ and $\theta_8(t)$ are mutually orthogonal but not of unit energy, to normalize them we have

$$\Phi_7(t) = \frac{\theta_7(t)}{|\theta_7|} \quad (\text{B.42})$$

$$\Phi_8(t) = \frac{\theta_8(t)}{|\theta_8|} \quad (\text{B.43})$$

where

$$|\theta_7| = \left[1 - b_{71}^2 - b_{72}^2 - b_{73}^2 - b_{74}^2 - b_{75}^2 - b_{76}^2 \right]^{1/2} \quad (\text{B.44})$$

$$|\theta_8| = \left[1 - b_{81}^2 - b_{82}^2 - b_{83}^2 - b_{84}^2 - b_{85}^2 - b_{86}^2 - b_{87}^2 \right]^{1/2} \quad (\text{B.45})$$

we have

$$\begin{aligned} b_{71} &= \int_0^T S_7(t) \Phi_1(t) dt \\ &= \int_0^T \left[\frac{2}{T} \right] \cos \left(\omega t - \frac{3\pi h t}{T} \right) \cos \left(\omega t + \frac{\pi h t}{T} \right) dt \end{aligned}$$

So $b_{71} = S_1$ (B.46)

$$\begin{aligned} b_{72} &= \int_0^T S_7(t) \Phi_2(t) dt \\ &= \int_0^T \left[\frac{2}{T} \right] \cos \left(\omega t - \frac{3\pi h t}{T} \right) \sin \left(\omega t + \frac{\pi h t}{T} \right) dt \\ &= \int_0^T \left[\frac{1}{T} \right] \sin \left[\frac{4\pi h t}{T} \right] dt = \frac{1 - \cos(4\pi h)}{4\pi h} = C_1 \end{aligned}$$

so, $b_{72} = C_1$ (B.47)

$$\begin{aligned} b_{73} &= \int_0^T S_7(t) \Phi_3(t) dt \\ &= \frac{1}{D_1} \left[\int_0^T S_7(t) S_3(t) dt - b_{31} b_{71} - b_{32} b_{72} \right] \quad (\text{B.48}) \end{aligned}$$

we have,

$$\int_0^T S_7(t) S_3(t) dt = \int_0^T \left[\frac{2}{T} \right] \cos \left(\omega t - \frac{3\pi h t}{T} \right) \cos \left(\omega t - \frac{\pi h t}{T} \right) dt$$

$$= \int_0^T \left[\frac{1}{T} \right] \cos \left[\frac{2\pi ht}{T} \right] dt = \frac{\sin(2\pi h)}{2\pi h} = S_o \quad (\text{B.49})$$

So putting b_{71} , b_{72} , b_{31} , b_{32} and equation (B.49) into the equation (B.48) we have

$$b_{73} = \frac{S_o - S_o S_1 - C_o C_1}{D_1} \quad (\text{B.50})$$

$$\begin{aligned} b_{74} &= \int_0^T S_7(t) \Phi_4(t) dt \\ &= \int_0^T S_7(t) \left[\frac{S_4(t) - b_{41} \Phi_1(t) - b_{42} \Phi_2(t)}{D_1} \right] dt \\ &= \frac{1}{D_1} \left[\int_0^T S_7(t) S_4(t) dt - b_{41} b_{71} - b_{42} b_{72} \right] \quad (\text{B.51}) \end{aligned}$$

we have

$$\begin{aligned} \int_0^T S_7(t) S_4(t) dt &= \int_0^T \left[\frac{2}{T} \right] \cos \left[\omega ct - \frac{3\pi ht}{T} \right] \sin \left[\omega ct - \frac{\pi ht}{T} \right] dt \\ &= \int_0^T \left[\frac{1}{T} \right] \sin \left[\frac{2\pi ht}{T} \right] dt = \frac{1 - \cos(2\pi h)}{2\pi h} = C_o \quad (\text{B.52}) \end{aligned}$$

by putting b_{71} , b_{72} , b_{41} , b_{42} and equation (B.52) in equation (B.51) we have

$$b_{74} = \frac{C_o + C_o S_1 - S_o C_1}{D_1} \quad (\text{B.53})$$

$$b_{75} = \int_0^T S_7(t) \Phi_5(t) dt$$

$$\begin{aligned}
&= \int_0^T S_7(t) \left[\frac{S_5(t) - b_{51}\Phi_1(t) - b_{52}\Phi_2(t) - b_{53}\Phi_3(t) - b_{54}\Phi_4(t)}{D_2} \right] dt \\
&= \frac{1}{D_2} \left[\int_0^T S_7(t) S_5(t) dt - b_{51}b_{71} - b_{52}b_{72} - b_{53}b_{73} - b_{54}b_{74} \right]
\end{aligned}$$

Here we have

$$\begin{aligned}
\int_0^T S_7(t) S_5(t) dt &= \int_0^T \left(\frac{2}{T} \right) \cos \left(\omega_c t - \frac{3\pi h t}{T} \right) \cos \left(\omega_c t + \frac{3\pi h t}{T} \right) dt \\
&= \int_0^T \left(\frac{1}{T} \right) \cos \left(\frac{6\pi h t}{T} \right) dt = \frac{\sin(6\pi h)}{6\pi h}
\end{aligned}$$

and define

$$S_2 = \frac{\sin(6\pi h)}{6\pi h} \quad (\text{B.55})$$

so we have

$$\int_0^T S_7(t) S_5(t) dt = S_2 \quad (\text{B.56})$$

by putting $b_{51}, b_{52}, b_{71}, b_{72}$ and equation (B.56) into equation (B.54) we have

$$b_{75} = \frac{S_2 - S_0 S_1 + C_0 C_1 - b_{53}b_{73} - b_{54}b_{74}}{D_2} \quad (\text{B.57})$$

$$b_{76} = \int_0^T S_7(t) \Phi_6(t) dt$$

$$= \int_0^T S_7(t) \left[\frac{S_6(t) - b_{61}\Phi_1(t) - b_{62}\Phi_2(t) - b_{63}\Phi_3(t) - b_{64}\Phi_4(t)}{D_2} \right] dt$$

$$= \frac{1}{D_2} \left[\int_0^T S_7(t) S_6(t) dt - b_{61} b_{71} - b_{62} b_{72} - b_{63} b_{73} - b_{64} b_{74} \right] \quad (B.58)$$

Here,

$$\begin{aligned} \int_0^T S_7(t) S_6(t) dt &= \int_0^T \left[\frac{2}{T} \right] \cos \left[\omega t - \frac{3\pi h t}{T} \right] \sin \left[\omega t + \frac{3\pi h t}{T} \right] dt \\ &= \int_0^T \left[\frac{1}{T} \right] \sin \left[\frac{6\pi h t}{T} \right] dt = \frac{1 - \cos(6\pi h)}{6\pi h} \end{aligned}$$

define

$$C_2 = \frac{1 - \cos(6\pi h)}{6\pi h} \quad (B.59)$$

we have

$$\int_0^T S_7(t) S_6(t) dt = C_2 \quad (B.60)$$

by putting $b_{61}, b_{62}, b_{71}, b_{72}$ and equation (B.60) into (B.58) and also by using (B.35) and (B.38) we have

$$b_{76} = \frac{C_2 - C_0 S_1 - S_0 C_1 + b_{54} b_{73} - b_{53} b_{74}}{D_2} \quad (B.61)$$

Now, putting b_{71} and b_{72} into equation (B.44) we have

$$|\theta_7| = \left[1 - C_1^2 - S_1^2 - b_{73}^2 - b_{74}^2 - b_{75}^2 - b_{76}^2 \right]^{1/2} \quad \text{and define}$$

$$D_3 = \left[1 - C_1^2 - S_1^2 - b_{73}^2 - b_{74}^2 - b_{75}^2 - b_{76}^2 \right]^{1/2} \quad (B.62)$$

so that $|\theta_7| = D_3$. And by using (B.40) in (B.42) we have

$$\begin{aligned} \Phi_7(t) &= \left[S_7(t) - S_1 \Phi_1(t) - C_1 \Phi_2(t) - b_{73} \Phi_3(t) - b_{74} \Phi_4(t) \right. \\ &\quad \left. - b_{75} \Phi_5(t) - b_{76} \Phi_6(t) \right] \frac{1}{D_3} \quad (B.63) \end{aligned}$$

For $\Phi_B(t)$ we have the coefficients,

$$\begin{aligned}
 b_{B1} &= \int_0^T S_B(t) \Phi_1(t) dt \\
 &= \int_0^T \left(\frac{2}{T}\right) \sin\left(\omega t - \frac{3\pi h t}{T}\right) \cos\left(\omega t + \frac{\pi h t}{T}\right) dt \\
 &= \int_0^T \left(\frac{1}{T}\right) \sin\left[-\frac{4\pi h t}{T}\right] dt = \frac{\cos(4\pi h) - 1}{4\pi h} = -C_1
 \end{aligned}$$

Then,

$$b_{B1} = -C_1 \quad (\text{B.64})$$

$$\begin{aligned}
 b_{B2} &= \int_0^T S_B(t) \Phi_2(t) dt \\
 &= \int_0^T \left(\frac{2}{T}\right) \sin\left(\omega t - \frac{3\pi h t}{T}\right) \sin\left(\omega t + \frac{\pi h t}{T}\right) dt \\
 &= \int_0^T \left(\frac{1}{T}\right) \cos\left[\frac{4\pi h t}{T}\right] dt = \frac{\sin(4\pi h)}{4\pi h}
 \end{aligned}$$

so

$$b_{B2} = S_1 \quad (\text{B.65})$$

$$\begin{aligned}
 b_{B3} &= \int_0^T S_B(t) \Phi_3(t) dt \\
 &= \int_0^T S_B(t) \left[\frac{S_3(t) - b_{31}\Phi_1(t) - b_{32}\Phi_2(t)}{D_1} \right] dt \\
 &= \frac{1}{D_1} \left[\int_0^T S_B(t) S_3(t) dt - b_{31}b_{B1} - b_{32}b_{B2} \right] \quad (\text{B.66})
 \end{aligned}$$

where,

$$\begin{aligned} \int_0^T S_8(t) S_3(t) dt &= \int_0^T \left(\frac{2}{T} \right) \sin \left(\omega t - \frac{3\pi h t}{T} \right) \cos \left(\omega t - \frac{\pi h t}{T} \right) dt \\ &= \int_0^T \left(\frac{1}{T} \right) \sin \left(-\frac{2\pi h t}{T} \right) dt = \frac{\cos(2\pi h) - 1}{2\pi h} = -C_o \end{aligned}$$

so,
$$\int_0^T S_8(t) S_3(t) dt = -C_o \quad (B.67)$$

By putting $b_{31}, b_{32}, b_{81}, b_{82}$ and (B.67) into (B.66) we have

$$b_{83} = \frac{-C_o + S_o C_1 - C_o S_1}{D_1} = -b_{74} \quad (B.68)$$

$$\begin{aligned} b_{84} &= \int_0^T S_7(t) \Phi_4(t) dt \\ &= \int_0^T S_8(t) \left[\frac{S_4(t) - b_{41} \Phi_1(t) - b_{42} \Phi_2(t)}{D_1} \right] dt \\ &= \frac{1}{D_1} \left[\int_0^T S_8(t) S_4(t) dt - b_{41} b_{81} - b_{42} b_{82} \right] \quad (B.69) \end{aligned}$$

we have

$$\begin{aligned} \int_0^T S_8(t) S_4(t) dt &= \int_0^T \left(\frac{2}{T} \right) \sin \left(\omega t - \frac{3\pi h t}{T} \right) \sin \left(\omega t - \frac{\pi h t}{T} \right) dt \\ &= \int_0^T \left(\frac{1}{T} \right) \cos \left(\frac{2\pi h t}{T} \right) dt = \frac{\sin(2\pi h)}{2\pi h} = S_o \end{aligned}$$

So
$$\int_0^T S_8(t) S_4(t) dt = S_o \quad (B.70)$$

By putting $b_{41}, b_{42}, b_{81}, b_{82}$ and (B.70) into (B.69)

$$b_{84} = \frac{S_0 - C_0 C_1 - S_0 S_1}{D_1} = b_{73} \quad (\text{B.71})$$

$$\begin{aligned} b_{85} &= \int_0^T S_8(t) \Phi_5(t) dt \\ &= \int_0^T S_8(t) \left[\frac{S_5(t) - b_{51}\Phi_1(t) - b_{52}\Phi_2(t) - b_{53}\Phi_3(t) - b_{54}\Phi_4(t)}{D_2} \right] dt \\ &= \frac{1}{D_2} \left[\int_0^T S_8(t) S_5(t) dt - b_{51}b_{81} - b_{52}b_{82} - b_{53}b_{83} - b_{54}b_{84} \right] \end{aligned}$$

Here we have

$$\begin{aligned} \int_0^T S_8(t) S_5(t) dt &= \int_0^T \left(\frac{2}{T} \right) \sin \left(\omega t - \frac{3\pi h t}{T} \right) \cos \left(\omega t + \frac{3\pi h t}{T} \right) dt \\ &= \int_0^T \left(\frac{1}{T} \right) \sin \left(-\frac{6\pi h t}{T} \right) dt = \frac{\cos(6\pi h) - 1}{6\pi h} = -C_2 \end{aligned}$$

$$\text{so,} \quad \int_0^T S_8(t) S_5(t) dt = -C_2 \quad (\text{B.73})$$

By putting $b_{51}, b_{52}, b_{81}, b_{82}$ and (B.68), (B.71), (B.73) into (B.72)

$$b_{85} = \frac{-C_2 + S_0 C_1 + C_0 S_1 + b_{53}b_{74} - b_{54}b_{73}}{D_2}$$

$$\text{So,} \quad b_{85} = -b_{76} \quad (\text{B.74})$$

$$b_{86} = \int_0^T S_8(t) \Phi_6(t) dt$$

$$\begin{aligned}
&= \int_0^T S_B(t) \left[\frac{S_6(t) - b_{61}\Phi_1(t) - b_{62}\Phi_2(t) - b_{63}\Phi_3(t) - b_{64}\Phi_4(t)}{D_2} \right] dt \\
&= \frac{1}{D_2} \left[\int_0^T S_B(t) S_6(t) dt - b_{61}b_{81} - b_{62}b_{82} - b_{63}b_{83} - b_{64}b_{84} \right] \quad (B.75)
\end{aligned}$$

Here,

$$\begin{aligned}
\int_0^T S_B(t) S_6(t) dt &= \int_0^T \left(\frac{2}{T} \right) \sin\left(\omega t - \frac{3\pi h t}{T}\right) \sin\left(\omega t + \frac{3\pi h t}{T}\right) dt \\
&= \int_0^T \left(\frac{1}{T} \right) \cos\left(\frac{6\pi h t}{T} \right) dt = \frac{\sin(6\pi h)}{6\pi h} = S_2
\end{aligned}$$

$$\text{So} \quad \int_0^T S_B(t) S_6(t) dt = S_2 \quad (B.76)$$

Now by putting, b_{61} , b_{62} , b_{81} , b_{82} and equations (B.35), (B.38), (B.68), (B.71), (B.76) into (B.75) we have

$$b_{86} = \frac{S_2 + C_0 C_1 - S_0 S_1 - b_{74}b_{54} - b_{53}b_{73}}{D_2}$$

$$\text{So} \quad b_{86} = b_{75} \quad (B.77)$$

$$b_{87} = \int_0^T S_B(t) \Phi_7(t) dt$$

By using (B.73) and remembering that $S_7(t)$ and $S_8(t)$ are orthogonal to each other

$$\begin{aligned}
b_{87} &= \frac{1}{D_3} \int_0^T S_B(t) \left[S_7(t) - S_1\Phi_1(t) - C_1\Phi_2(t) - b_{73}\Phi_3(t) \right. \\
&\quad \left. - b_{74}\Phi_4(t) - b_{75}\Phi_5(t) - b_{76}\Phi_6(t) \right] dt
\end{aligned}$$

$$= \frac{1}{D_3} \left[-b_{81}s_1 - c_1 b_{82} - b_{73}b_{83} - b_{74}b_{84} - b_{75}b_{85} - b_{76}b_{86} \right]$$

By inserting b_{81}, \dots, b_{86} and b_{73}, \dots, b_{76} into the above equation we get

$$b_{87} = 0 \quad (B.78)$$

Now, we need $|\theta_8|$ to write the equation for $\Phi_8(t)$, so by using (B.45) and putting b_{81} and b_{82} into this equation

$$|\theta_8| = \left[1 - c_1^2 - s_1^2 - b_{83}^2 - b_{84}^2 - b_{85}^2 - b_{86}^2 - b_{87}^2 \right]^{1/2}$$

$$\text{So,} \quad |\theta_8| = D_3 \quad (B.79)$$

as it is seen from (B.62).

So $\Phi_8(t)$ can now be written by using equations (B.41) and (B.43); we also use equations (B.64), (B.65), (B.68), (B.71), (B.74), (B.77), (B.78) and (B.79) for the coefficients $b_{81}, b_{82}, \dots, b_{87}, |\theta_8|$ respectively. So finally

$$\begin{aligned} \Phi_8(t) = \frac{1}{D_3} \left[s_8(t) + c_1 \Phi_1(t) - s_1 \Phi_2(t) + b_{74} \Phi_3(t) - b_{73} \Phi_4(t) \right. \\ \left. + b_{76} \Phi_5(t) - b_{75} \Phi_6(t) \right] \quad (B.80) \end{aligned}$$

Now, the eight dimensional orthonormal basis $\{\Phi_1(t), \Phi_2(t), \dots, \Phi_8(t)\}$ have been constructed by using the Gram-Schmidt procedure.